Investigation of Sleep Neural Dynamics in Intracranial EEG Patients

Sparsh Jain

Thesis submitted to the Faculty of the
Virginia Polytechnic Institute and State University
in partial fulfillment of the requirements for the degree of

Master of Science
in
Biomedical Engineering

Sujith Vijayan, Chair
Matthew Buczynski
Ann Gregus

May 07, 2021
Blacksburg, Virginia

Keywords: Sleep staging, electrode localization, electrophysiology, oscillations, iEEG, alpha activity

Investigation of Sleep Neural Dynamics in Intracranial EEG Patients

Sparsh Jain

(ABSTRACT)

Intracranial electroencephalography (iEEG) provides superior diagnostic and research benefits over non-invasive EEG in terms of spatial resolution and the level of electrophysiological detail. Post-operative Computed Tomography (CT) scans provide the precision in electrode localization required for clinical purposes; however, to use this data for basic sleep research the challenge lies in identifying the precise locations of the implanted electrodes' recording sites in terms of neuroanatomical regions as well as reliable scoring of their sleep data without the aid of facial electrodes. While existing methods can be combined to determine their exact locations in three-dimensional space, they fail to identify the functionally relevant gray matter areas that lie closest to them, especially if the points lie in the white matter. We introduce an iterative sphere inflation algorithm in conjunction with a unified pipeline to detect the exact as well as nearest regions of interest for these recording sites. Next, for sleep scoring purposes, we establish differences observed in alpha band activity between wakefulness and rapid eye movement (REM) sleep in frontal and temporal regions of iEEG patients. Lastly, we implement an automated sleep scoring method relying on the variations in alpha and delta bands power during sleep which can be applied to large sets of iEEG data recorded without accompanying electrooculogram (EOG) and electromyogram (EMG) electrodes available across labs for use in studies pertaining to neural dynamics during sleep.

Investigation of Sleep Neural Dynamics in Intracranial EEG Patients

Sparsh Jain

(GENERAL AUDIENCE ABSTRACT)

Patients with epilepsy (a neurological disorder characterized by seizures) who do not respond to medication often undergo invasive monitoring of their brains' electrical activity using intracranial electroencephalography (iEEG). iEEG requires a surgery in which electrodes are inserted directly into the patient's brain for better measurements. While they are monitored, these patients offer a unique opportunity for research studies that investigate the role of sleep in various learning, memory mechanisms and other health-related areas. This is because the direct contact of the electrodes with the brain tissue provides far superior quality and resolution of brain activity data in comparison to non-invasive cap-based EEG that healthy subjects wear over their scalp. However, in order to derive meaningful conclusions from these invasive recordings, we must first know the exact areas of the brain from which each site records the electrical data. We must then be able to identify which stage of sleep the patient is in at any given point in time, to be able to successfully correlate specific sleep stage-related activity with our research objectives; these patients often lack the facial electrodes used for standard sleep scoring procedures. To solve the first problem, we present an electrode localization method along with an algorithm to determine which neighboring regions contribute most to a given site's recorded data. For the second problem, we first establish a difference in the behavior of alpha waves in the brain between wakefulness and rapid eye movement (REM) sleep. Lastly, we present an automated method to classify sleep data into different stages based on the variation in alpha waves and delta waves found during sleep.

Dedication

This work is dedicated to the 50 million people suffering from epilepsy, as well as the clinicians and neuroscientists working tirelessly to find a cure.

Acknowledgments

First, I would like to thank my advisor, Dr. Sujith Vijayan, and my committee members Dr. Ann Gregus and Dr. Matthew Buczynski for their guidance and encouragement.

I would also like to thank my fellow lab members Andrew and Pat, the Epilepsy Monitoring Unit, and Dr. Mark Witcher from the Department of Neurosurgery at Carilion Roanoke Memorial Hospital for their assistance. I am also very thankful to our patients who volunteered for our studies, and to Dr. Roan LaPlante for his creation and assistance with the IELU pipeline.

I shall remain deeply indebted to my wonderful teachers at St. Lawrence High School, as well as my undergraduate mentors, Dr. Rajib Bandyopadhyay and Dr. Ratna Ghosh. The knowledge, skills and values which they imparted have been instrumental in making me a better student, engineer and researcher.

I feel extremely fortunate to have found amazing friends in graduate school. I would like to express my deepest gratitude to Gavin, Troy, Tré, Giovanni, Andrew, Pat, Kenneth, Connor, Keaton, Micah, Mark, Ryan, Sarah and Hannah for being sources of unwavering strength, inspiration and love through the many ups and downs of conducting research.

I wholeheartedly thank Amanda Covey for her constant words of motivation, guidance and for ensuring that I kept moving forward while maintaining good mental and emotional health. Her sheer warmth and willingness to be there made this journey significantly easier.

In the end, I would like to thank my parents and grandparents for their selfless love, guidance and sacrifices, without which I could not have achieved my goals. I have also been privileged to have my extended family's support and affection, both here in the States as well as from back home.

Contents

List of Figures

List of Tables

List of Abbreviations

AASM American Academy for Sleep Medicine

CT Computed Tomography

EEG Electroencephalogram

EMG Electromyogram

EOG Electrooculogram

IELU Interactive Electrode Localization Utility

LAMF Low-Amplitude Mixed-Frequency Signal

MRI Magnetic Resonance Imaging

RAS Right-Anterior-Superior Coordinate System

REM Rapid Eye Movement

Chapter 1

Introduction

1.1 Epilepsy

Epilepsy is one of the most common neurological disorders, which affects roughly 1% of the total world population, with an incidence of 2 million cases every year[41]. Epilepsy is characterized by seizures, which are caused by abnormal highly synchronous electrical discharge of neurons in the brain[26]. Depending on the type and severity, epilepsy causes a significant impact on the individual's quality of life, affecting both productivity and independence[62, 5]. While one or more of the 20 clinically approved anti-epileptic drugs successfully treat the condition in 2/3rd of the patient population, the remaining patients do not respond to medication. This type of epilepsy is called refractory epilepsy[37] and is most commonly present when the seizure activity originates from a specific region in the brain called the epileptic focus, as opposed to being spread throughout the brain. Temporal lobe epilepsy (TLE) accounts for a majority of such cases, and also makes up for 60% of all epilepsy cases . TLE is often associated with increased mortality[5], lower quality of life and a higher risk of cognitive impairments due to frequent seizures[21]. The common points of origin of seizure activity for TLE are the hippocampus and its surrounding areas.

1.2 EEG and Intracranial EEG

A vital step towards effective treatment of drug resistant epilepsy is the localization of the epileptic foci in the patient's brain[38]. This is achieved in two steps: First, non-invasive tests like conventional electroencephalography (EEG; see Fig. 1.5) and Magnetic Resonance Imaging (MRI, see Fig. 1.3) are conducted to gain preliminary information[61]. EEG might help detect abnormal electrical activity in specific regions and therefore help provide a general idea of where the epileptic foci may lie. MRI can help detect or rule out pathological tissue like lesions or tumors and provide an anatomical overview. Once the epileptologist has this set of information, intracranial electroencephalography (iEEG) is used to pinpoint the origin of the epileptic activity. iEEG consists of an invasive surgical procedure where electrodes are implanted in the subdural or subcortical regions of the brain. Fig. 1.1 and Fig. 1.2 show the implantation of grids, and grids as well as depth electrodes respectively. Subcortical grids, depth electrodes or a combination of both are used at the epileptologist's discretion. The patient is then weaned off anti-epileptic drugs while being continuously monitored for seizures and inter-ictal activity. Electrophysiological recordings from these electrodes are analyzed to determine the location and boundary of the affected gray matter and white matter regions[2]. Once there is conclusive data, a second surgery is performed to map the afflicted area(s) for necessary brain function as well as to explant the electrodes. Eventually, the neurosurgeon performs a final surgery to either resect the pathological brain tissue[3] or to implant a deep brain stimulator[7]. Hence, iEEG monitoring serves as a crucial step in treating many drug resistant epilepsy cases[2].

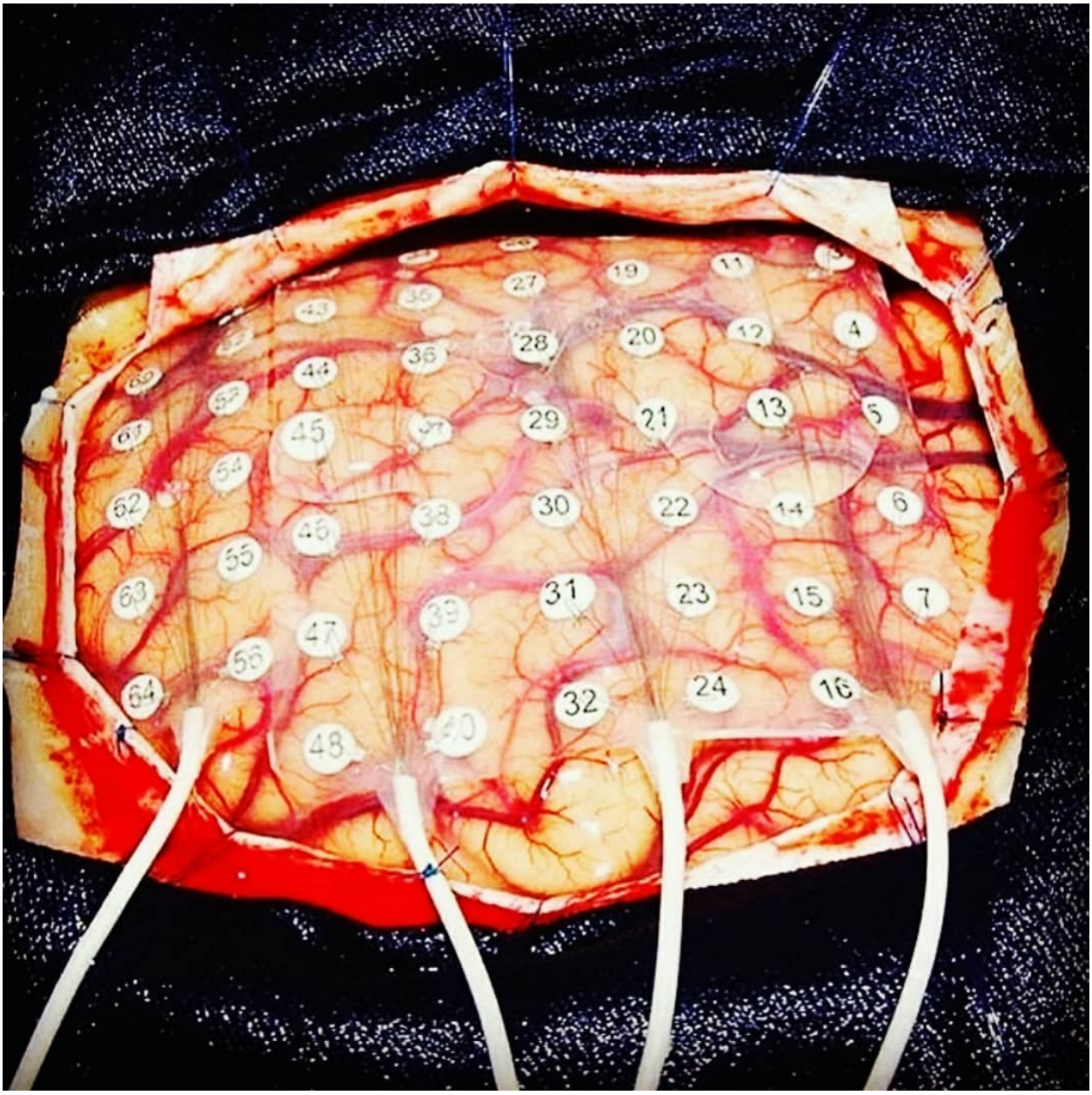

Figure 1.1: Placement of Grid Electrodes

1.2.1 Advantages of iEEG over conventional EEG

While conventional EEG is sufficient for diagnosing many neurological disorders and other illnesses, it suffers from low spatial resolution[23]. The electrical activity in the brain is primarily comprised of synchronized postsynaptic potentials generated in the pyramidal neurons. Millions of neurons project these electric potentials through the neocortex which then arrive at the cortical surface[30]. When conventional EEG is used, these electrical signals are picked up by the scalp electrodes after they pass through the skull and meninges, thereby suffering from significant attenuation and noise[54]. Furthermore, volume conduction effect is another huge factor in the recordings obtained from this method. The recordings picked up by each electrode comprises of signals generated by different sets of large areas of the brain that are overlapped and mixed with one another as they flow through the skull. This greatly decreases the spatial resolution i.e., uniqueness of the electrical activity recorded at any given electrode[38]. Therefore, scalp EEG recordings a) fail to faithfully represent electrical activity generated by smaller populations of neurons that lie deeper inside the brain, and b) offer poor spatial resolution because of the volume conduction effect. This makes conventional EEG a poor choice as a final diagnostic test for these patients. iEEG on the other hand records electrical activity directly from the surface of the cortex (in case of subdural grids) and also from the deep-brain structures like the hippocampus, amygdala and other small neuronal populations owing to their finer recording sites[56]. This also bypasses the meninges as well as the skull, thereby preventing some signal attenuation. For research purposes[51], iEEG is the advantage of detecting electrical activity at much higher frequencies (up to 300Hz) compared to conventional EEG (up to 50 Hz)[34].

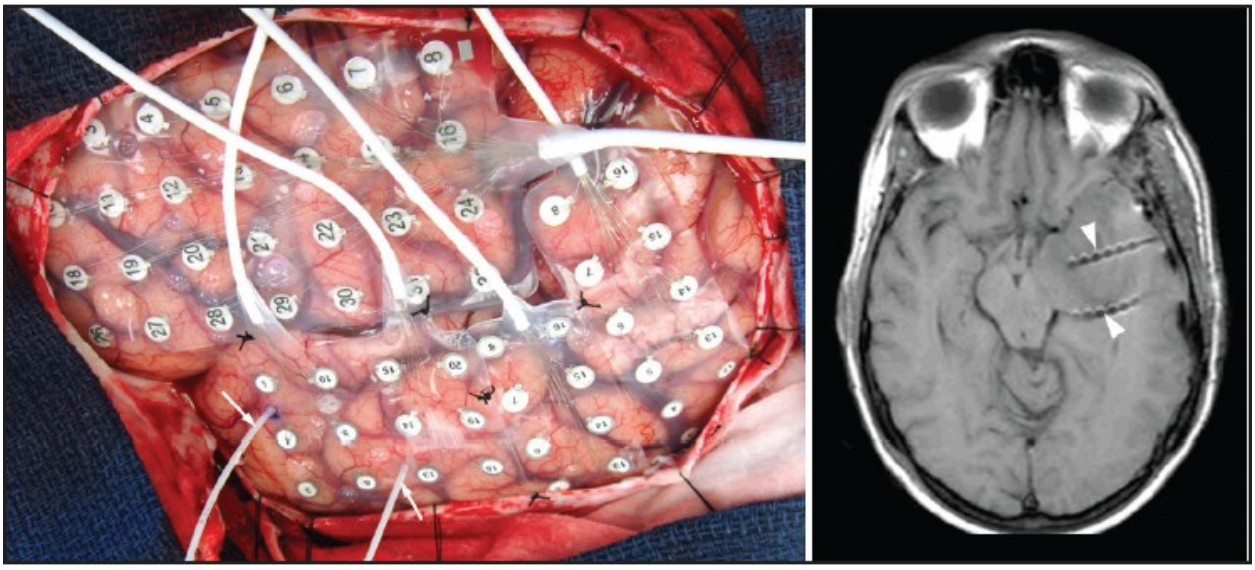

Figure 1.2: Placement of Grids and Depth Electrodes (Right: CT Scan)

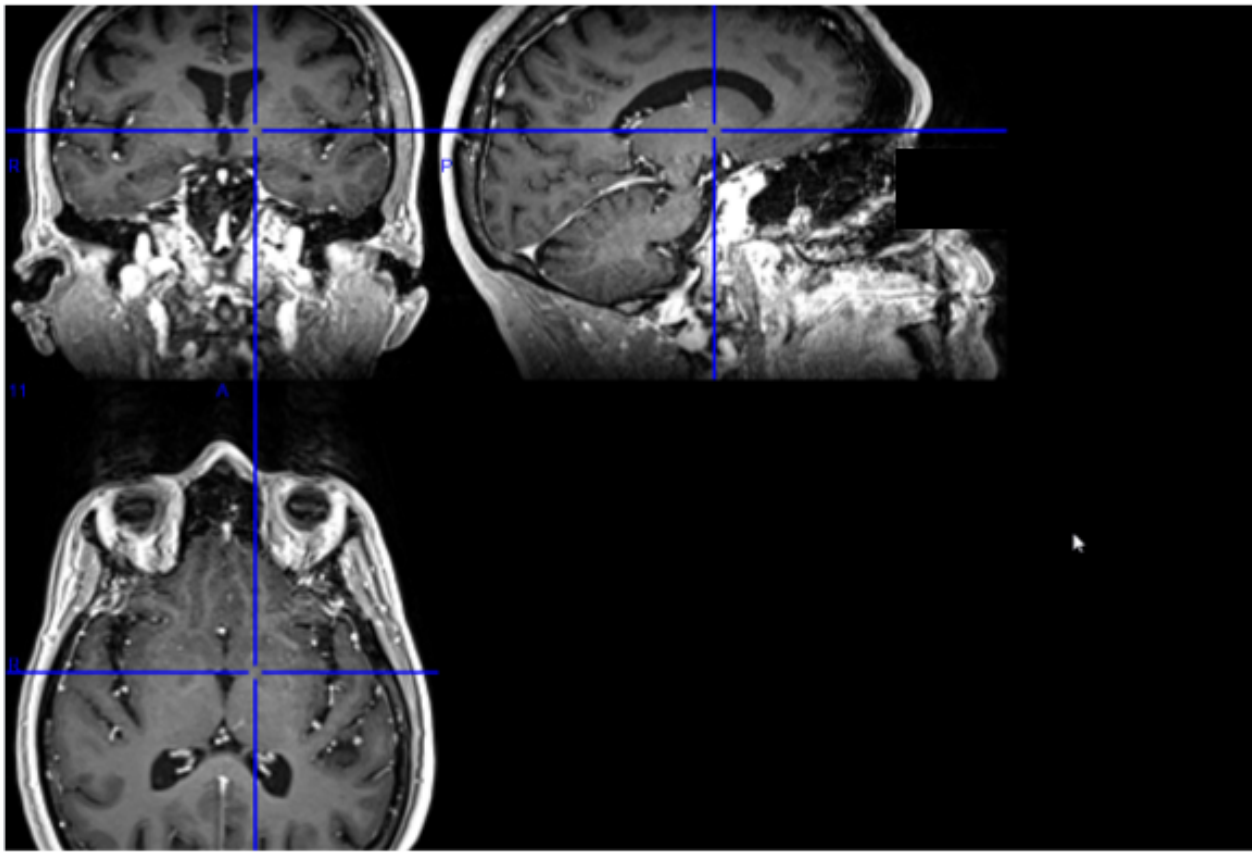

Figure 1.3: Pre-operative MRI

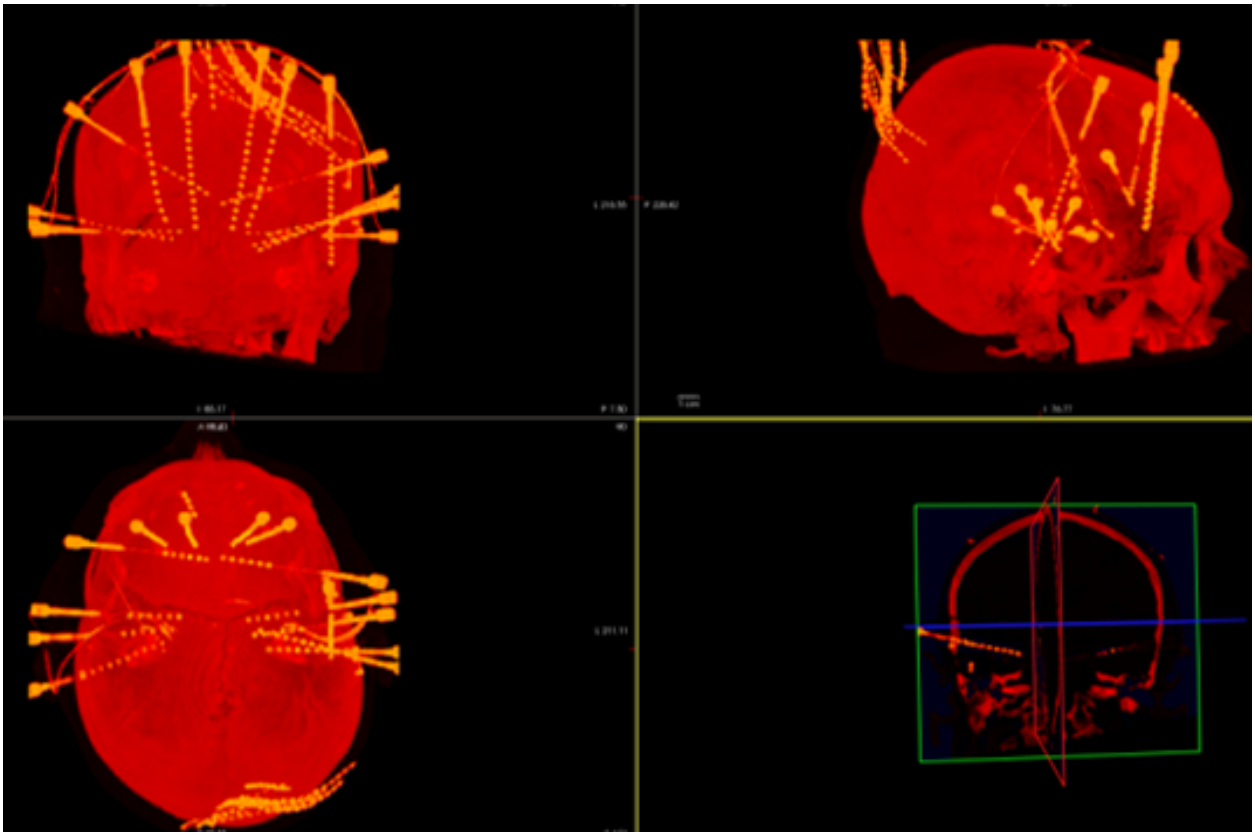

Figure 1.4: Post-operative CT

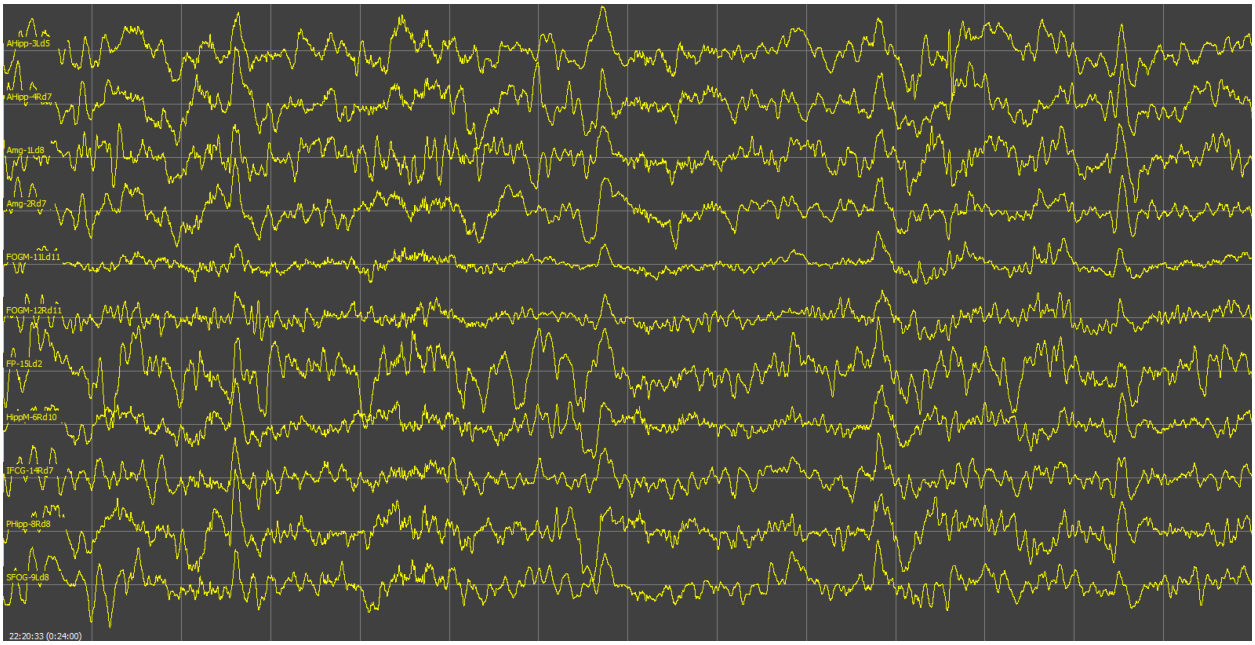

Figure 1.5: Sample EEG Recording

1.3 Brain Waves during Sleep

The human brain generates rhythmic electrical oscillations across a wide range of frequency[27]. A few of these waves are of special interest while investigating various memory and learning mechanisms as well as for sleep related studies[53],[4].

Delta waves are slow, large-amplitude (at least 75uV) oscillations that are typically present during N3 sleep (commonly referred to as deep or restorative sleep)[29, 27]. These waves are most prominent in the frontal regions of the brain and are often associated with processing of specific types of memory and learning during sleep. During N3 sleep, delta waves occupy at least 20% of the duration (see Fig. 1.12. Infants typically have a lot more delta activity during sleep than adults, and the amount of delta waves usually decreases with age[59].

Theta waves are rhythmic oscillations of 4-8Hz found in the hippocampal as well as cortical regions. Hippocampal theta waves are believed to be associated with memory formation processes. They are also observed during transition from wakefulness to N1 sleep (along with a decrease in alpha activity) and during REM sleep[59].

Alpha waves are oscillations between 8-12Hz and are most prominent in the occipital regions during eyes-closed wakefulness (see Fig. 1.6). For sleep scoring purposes, presence of alpha activity in the occipital regions is typically used to determine if the subject is awake or not. As the sleep transitions into N1 stage, alpha activity attenuates and is replaced by low amplitude mixed frequency signals[33]. Alpha activity also decreases when the subject opens their eyes. Historically, alpha waves were associated with idleness and lack of cortical activity but it is now believed that they play a key role in selective activation and deactivation of different cortical networks in order to facilitate specific neural processes during sleep[46, 59, 49, 14].

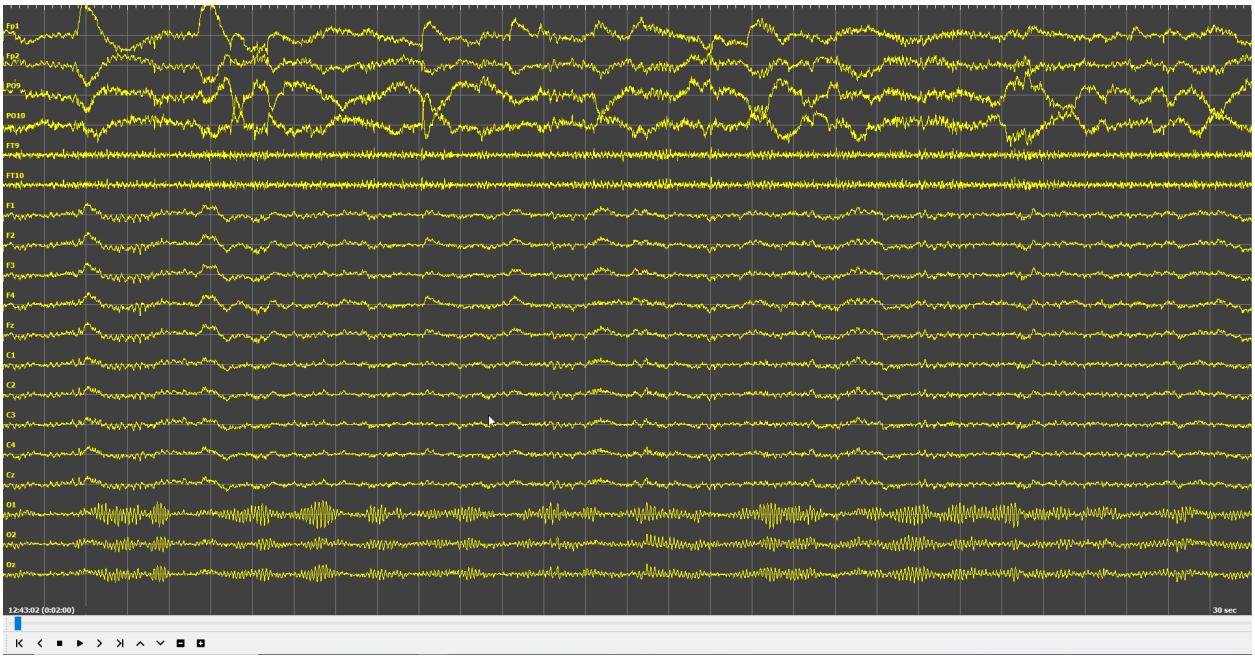

Figure 1.6: Alpha power in occipital channels during W (Conventional EEG)

1.4 Sleep Stages and Scoring

A typical sleep session consists of the subject transitioning between different sleep stages in cycles. The AASM classifies sleep into the following stages- Wake (W), Non-REM 1, 2, 3 (N1, N2, N3), and Rapid Eye Movement (REM) sleep[33].

Stage W is defined as the subject being fully awake and conscious (see Fig. 1.7, 1.8). During eyes-closed wakefulness, alpha activity can be typically observed in the occipital regions.

Stage N1 or light sleep is the transitional stage where the subject is no longer awake but can be aroused easily (see Fig. 1.9). Typically, alpha activity in the occipital regions diminishes and is replaced by a more global low-amplitude mixed-frequency (LAMF) signal[47].

Stage N2 is characterized by K-complexes (sharp deflections in signal amplitude, promi-

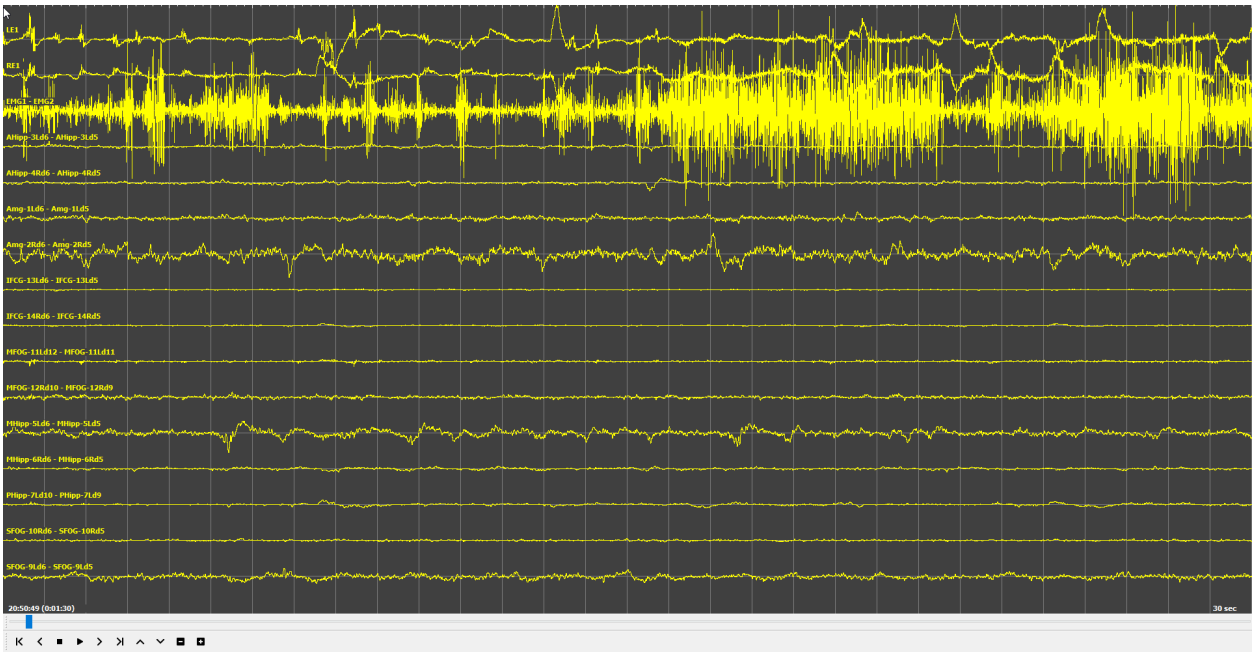

Figure 1.7: A W epoch with high muscle tone (Intracranial EEG)

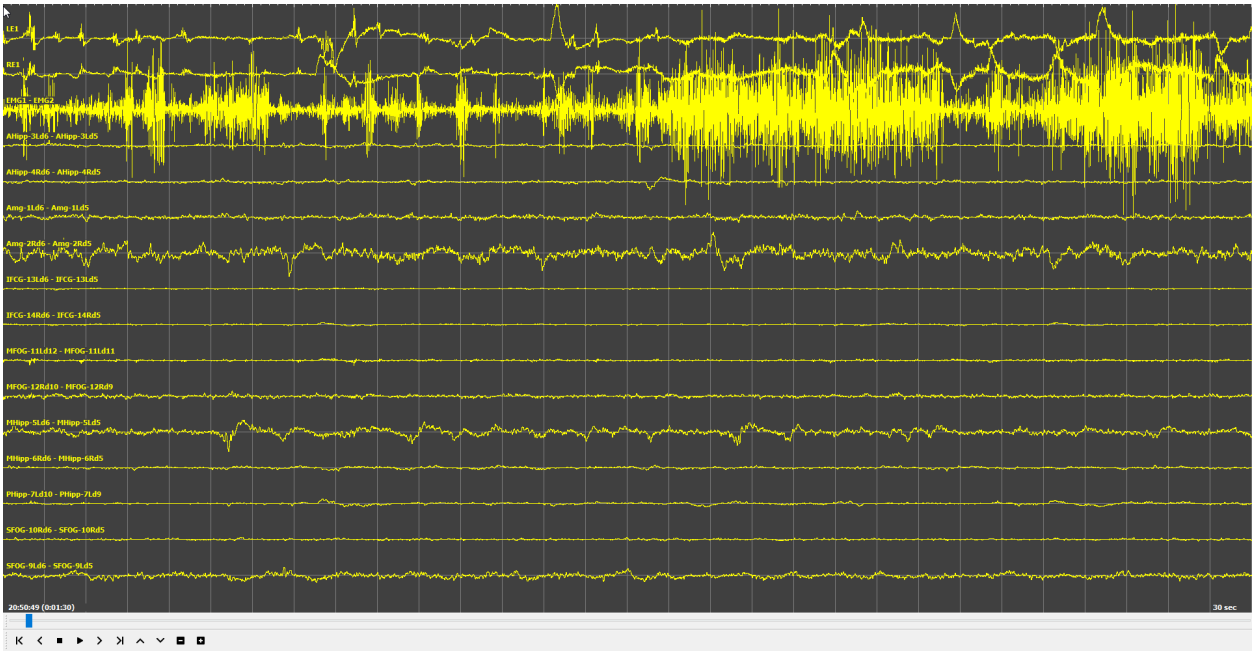

Figure 1.8: A W epoch with prominent alpha activity and high muscle tone (Conventional EEG)

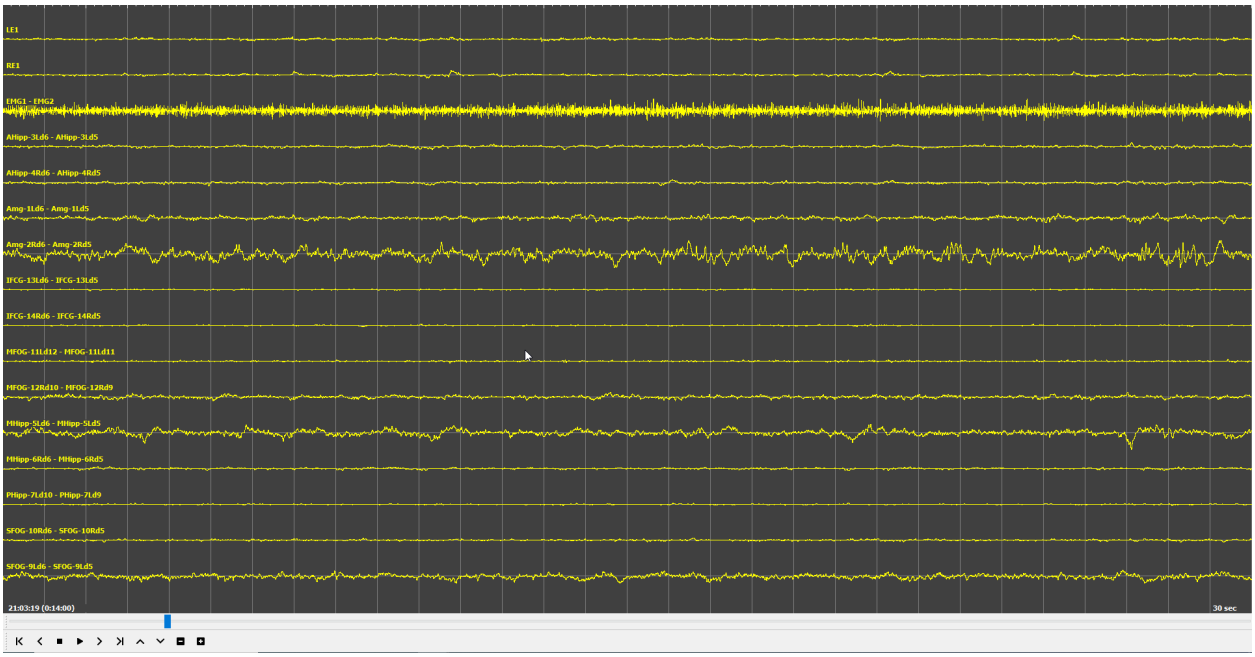

Figure 1.9: An N1 epoch with LAMF

nent in the frontal regions) and/or sleep spindles (rhythmic spindle-like oscillations between 11-16Hz strongest in the central regions) with low muscle tone[33, 12, 52] (see Fig. 1.10, 1.11).

Stage N3 or Delta sleep is characterized by delta wave formations in the frontal regions and typically follows N2 sleep (see Fig. 1.12). At least 20% of N3 sleep consists of delta wave

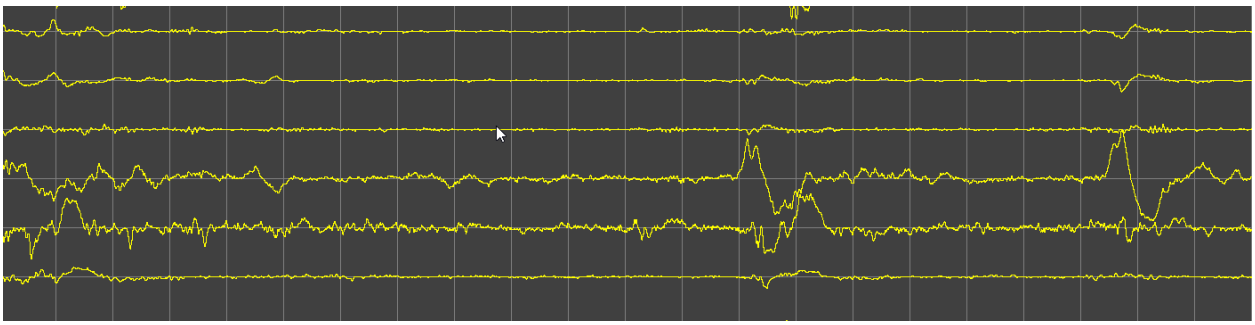

Figure 1.10: An N2 epoch with K-complexes

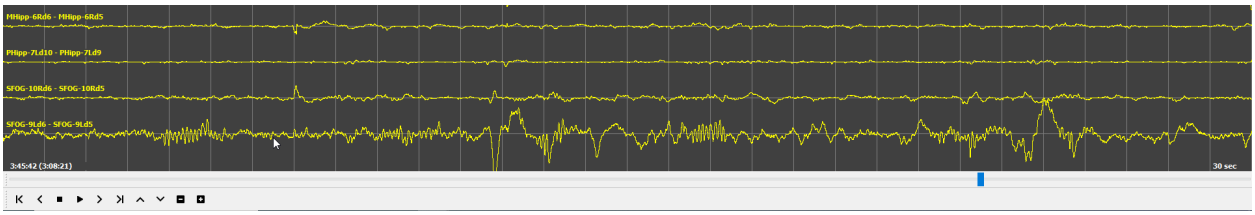

Figure 1.11: An N2 epoch with sleep spindles

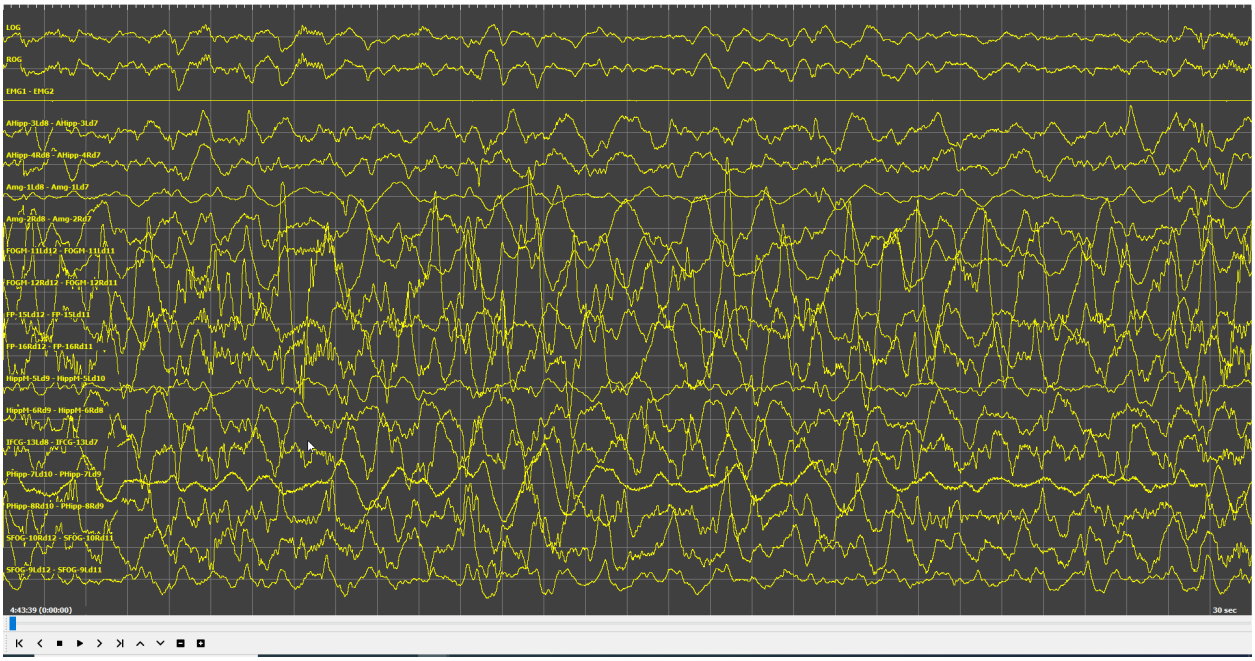

Figure 1.12: An N3 epoch with large delta waves

activity. It is the deepest stage of sleep[29, 58, 55].

Stage REM or rapid eye movement sleep comprises of the tonic part where rapid (conjugate) eye movements are prevalent along with muscle twitches and the phasic part where LAMF and low muscle tone (low chin EMG) are observed (see Fig. 1.13). Certain learning and memory processes are also executed during REM sleep[45, 57, 9].

A typical night's sleep comprises of 4-6 sleep cycles with about 20% time spent in N3 sleep.

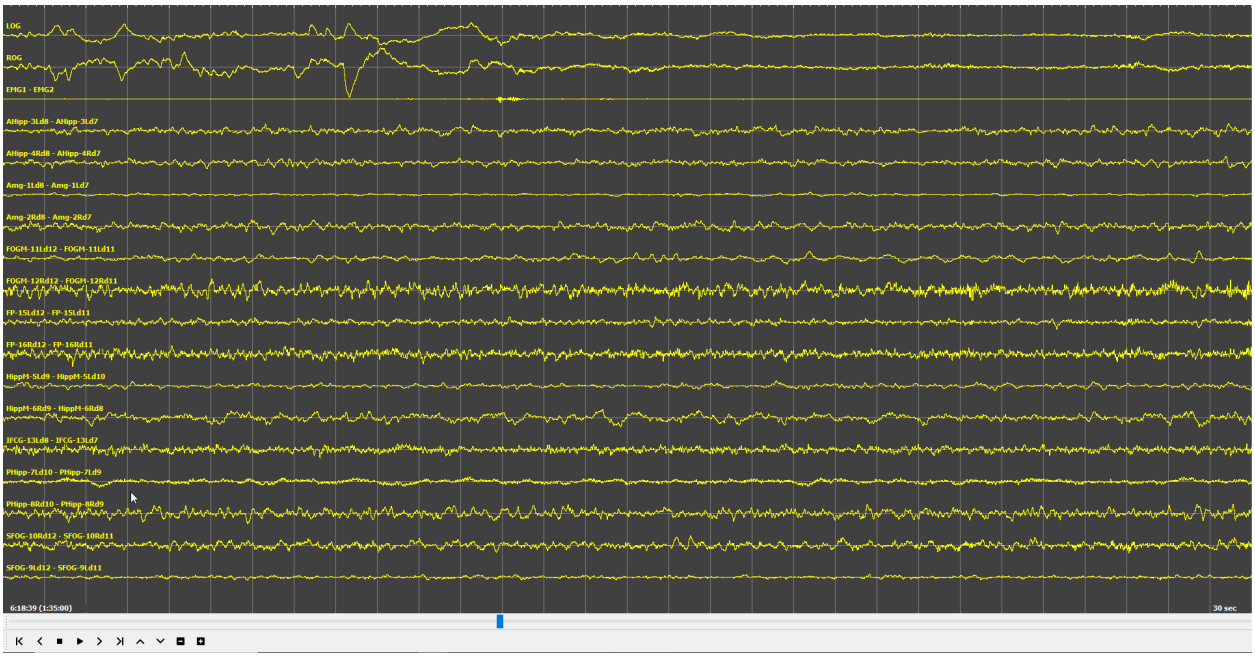

Figure 1.13: A REM epoch with conjugate eye movements in EOG

As the sleep progresses, REM duration increases per cycle and N3 duration decreases[47, 50] (see Fig. 1.14).

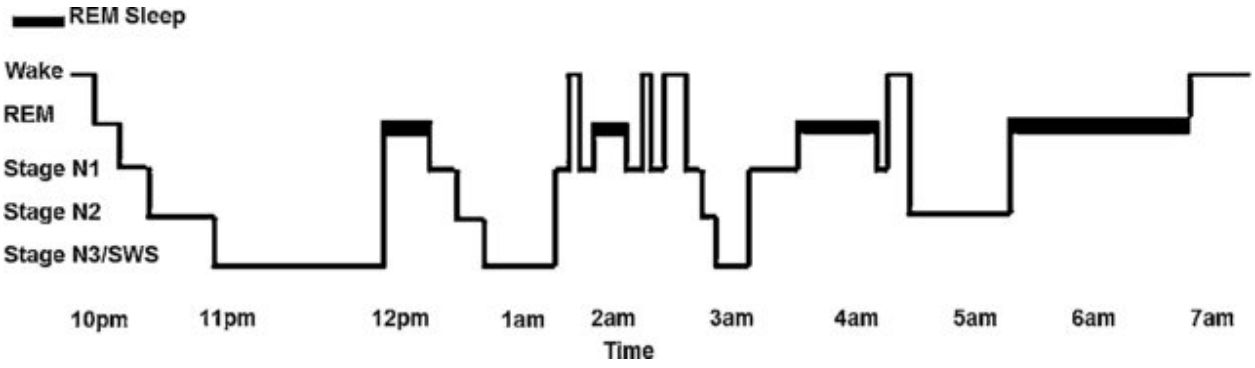

Figure 1.14: Hypnogram

1.5 Summary

A large number of sleep studies across the world focus on investigating various neural dynamics that govern learning and memory mechanisms during the different stages of sleep. While most of the data is collected from healthy volunteer subjects who undergo conventional EEG monitoring while performing different memory related tasks and sleeping, the inherent limitations of non-invasive EEG i.e., poor spatial resolution due to volume conduction effect as well as high signal attenuation are a huge impediment in detecting finer changes in local field potentials corresponding to smaller neuronal populations or structures that reside deep underneath the cortex. As a result, a lot of these studies also target clinical patients that undergo invasive EEG monitoring as described in the previous sections[15, 39]. The iEEG setup provides a much cleaner, robust, and unique data set that can be attributed to relatively smaller regions of interest. However, to meaningfully use these EEG data sets, it is first necessary to i) estimate the dominant source(s) of activity picked up by each recording site (i.e., localization of recording sites to the nearest gray matter region of interest), and ii) accurately classify sleep data into different stages in order to investigate the neural dynamics associated with learning and memory mechanisms that are dependent on specific sleep stages. The latter is a particularly tricky problem because while the traditional sleep scoring method relies almost entirely on supplementary facial (eye and chin) electrodes to measure ocular as well as myographic activity, most existing iEEG recordings at clinical sites across the world consist of only the subdural and subcortical channels without the use of any EOG or EMG electrodes.

In chapter 2, we present our localization method along with the anatomical labelling algorithm to solve the first problem. In chapters 3 and 4, we present an automated method to score iEEG sleep data accurately without the use of EOG or EMG data.

Chapter 2

Electrode Localization

2.1 Introduction

Patients suffering from drug-resistant epilepsy form a large portion of the human subjects' group that undergo our research studies. These patients undergo surgery to have invasive electrodes (depth electrodes as well as cortical grids containing multiple individual recording sites called contact points) implanted in their brains for the purpose of electrophysiological measurements[39]. For our research, we investigate the recordings for various neural dynamics during sleep and wake periods. In order to derive meaningful inferences, it is necessary to know which gray matter regions are contributing to the activity measured by a given contact point.

On the clinical side, the epileptologist determines the number and spatial distribution of these electrodes in order to locate and outline the epileptic focus[2]. While the neurosurgeon has an approximate idea of the implanted electrodes' locations after the surgery is concluded, there is a certain degree of imprecision in estimating the exact anatomical location of each contact point. Moreover, post-operative inflammation and bleeding may shift the electrodes slightly from their initial locations. For example, a particular temporal electrode implanted in the anterior hippocampus has six contact points. Of these six points, only the first two contact points might end up residing in the hippocampus while the third, fourth and fifth

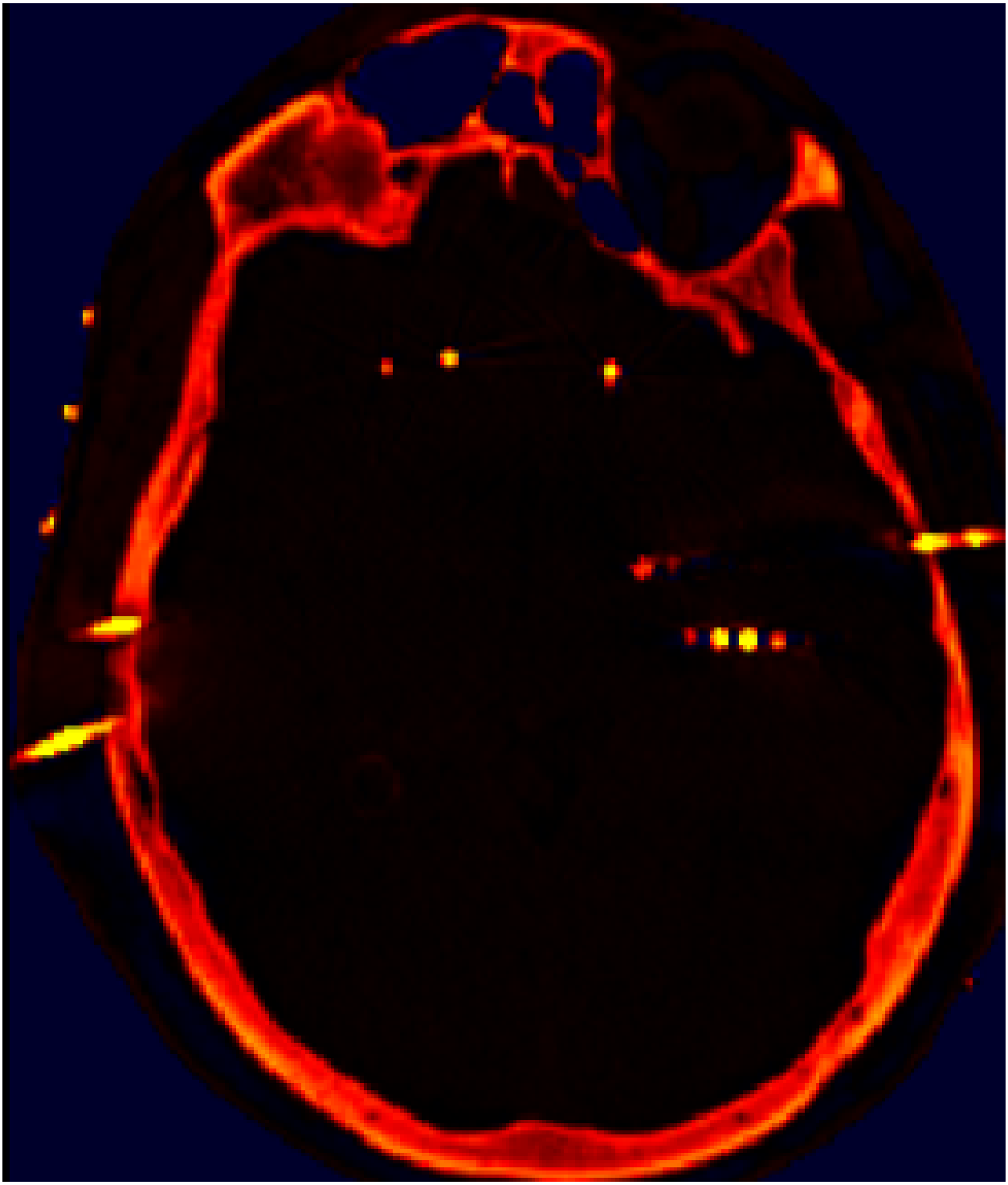

Figure 2.1: A post-operative CT scan overlayed with a heat colormap. The bright red dots represent the contact points lying on a particular axial slice

contact points all lie in the surrounding white matter, and the sixth contact point may lie in the skull. While the post-operative CT scan of the patient's brain may show that this electrode lies roughly in the hippocampal area, it is difficult to ascertain in which region each contact point lies (see Fig. 2.1).

To localize these contact points, the pre-operative MRI scan (see Fig. 2.2) is first converted into a three-dimensional brain volume from which various regions are extracted. This data is then aligned to the detailed anatomical map of an average human brain and adjustments are made based on the patient's specific parameters. Lastly, the entire gray matter is parcellated into sub-cortical and cortical regions of interest with well-defined boundaries. Additionally, other structures like ventricles, white matter and bone are also demarcated (see Fig. 2.4).

Once the patient's brain is successfully sub-divided into different anatomical regions, the post-operative CT scan[32, 8] is superimposed onto the MRI in order to visualize where the electrodes lie. Thus, by combining the anatomical information from the MRI and the actual electrode locations from the CT scan, we determine the exact anatomical location of each electrode contact point.

A number of pipelines have been developed by researchers to implement this in separate steps[25, 16, 24, 22, 20, 40, 36]; however, there are various drawbacks and difficulties associated with each of them. Based on the current literature, we present a unified pipeline that streamlines the entire process to achieve the goal of electrode localization. More importantly, we extend this work by creating a means of determining where these contact points lie within a volume. We do this for two reasons:

1. There is some uncertainty associated with a contact point's estimated location in the three-dimensional space, and

2. Contact points that lie in the white matter pick up electrical activity from nearby gray matter regions.

It is therefore important to determine which anatomical regions might be contributing to

the signal picked up by such contact points.

We accomplish this task by implementing an inflated-sphere algorithm in MATLAB[31], where a sphere is incrementally inflated around each contact point. Next, points lying on the surface of this sphere are located in space and their anatomical locations are recorded. By repeating this process while gradually increasing the radius of the sphere, the algorithm determines each unique gray matter region that lies successively closest to the contact point under consideration.

2.1.1 Sequence

1. The patient undergoes an MRI scan. This gives us the anatomical data.
2. The patient undergoes surgery and metal electrodes are implanted in their brain.
3. The patient undergoes a post-op CT scan. MRI cannot be used because the electrodes are metallic. This CT scan gives us an idea of where the electrodes are inside the brain.
4. We obtain the scan data from the hospital and execute the localization process.

2.1.2 Aim

We need to determine which anatomical region does each electrode contact point reside in (see Fig. 2.5, 2.6). For this, we need to find the 3D coordinates (called RAS coordinates: Right, Anterior and Superior) of each contact point. Once we have these coordinates, we use the MRI scans to find out which anatomical regions these points belong to. MRI gives us a much better resolution and detailed images of the various regions in the gray and white matter[61]. CT scan is a lot weaker in terms of outlining the various brain structures, and for our purpose only gives the location of the electrodes (metal shines brightly in CT scan

images).

2.2 Steps

1. MRI data: We use dcm2nii software[6] to combine all the 2D MRI images (DICOM files[28]) into an accurate 3D brain volume file.
Next, we use Freesurfer to work on this 3D volume to parcellate and segment the volume into different anatomical regions using a process called Reconstruction. This process gives us a colormap of the brain using brain atlases[20, 22, 24]. This colormap divides the subject's brain into a few hundred labels (e.g., hippocampus, amygdala etc.). Once this is done, we need to combine this MRI volume with the CT scan images so that we can superimpose the electrode contact points onto the MRI volume.
2. CT data: We use dcm2nii to combine all the 2D CT images into a 3D brain volume file. We then use the IELU software to superimpose the CT volume onto the MRI volume accurately using a process called co-registration. As mentioned earlier, we get the anatomical location and coordinate axes data from the MRI volume, and the electrode coordinates from the CT volume. Once co-registration is done, we get a combined volume as output file with red dots denoting each contact point that the algorithm automatically detects. Clicking on these dots gives us the RAS coordinates.

As a reminder, we need the MRI data to generate the colormap for the anatomical regions (e.g. hippocampus) as well as get the coordinate axes. Next, we need the CT scan to know where exactly in the above volume each contact point lies. The electrode image comes from the CT scan, which is done post operatively.

Analogy: We have the following two data sets:

a) Map of a city the names of places along with their zip codes, latitudes, and longitudes
b) A large picture of the aerial view of this city, same in size as the map. The picture has 5 places marked with red dots, corresponding to five shops (e.g. KFC).
Our Ultimate Goal: To find out the coordinates and zip codes for these five marked places. For this, we need to overlay the giant picture onto the map accurately. Once we do this, we can find out the coordinates of each red dot. Ultimately, we can find out the zip code / area name too.
Here, the city map (a) is equivalent to the patient's MRI scans. The MRI volume gives us the structural and anatomical information about the brain, but it does not have the electrodes yet (red dots). The giant picture of the physical city (b) is the patient's CT scans. It does not give us a high-resolution description of the city, but it has the five places of interest marked with red dots (same as the electrode contact points that light up on the CT scan). Therefore, these red dots represent the electrode contact points. The zip codes or area names represent the different anatomical labels in the brain i.e., Hippocampus, Amygdala etc. By combining (a) and (b) we create a unified map that tells us what the coordinates for each point of interest are. This overlaying is achieved by Co-registration using the IELU software, whereas the map (a) itself is constructed using Reconstruction (FreeSurfer software). During reconstruction, the software constructs an accurate volume of the brain (= city map with coordinates) and then divides this map into different areas (= anatomical labels like amygdala etc.).

2.3 Pipeline

1. During a CT / MRI scan, a number of two-dimensional slices/ images of the brain are taken in DICOM format. These slices are taken about 1 to 2 mm apart. For the pipeline,

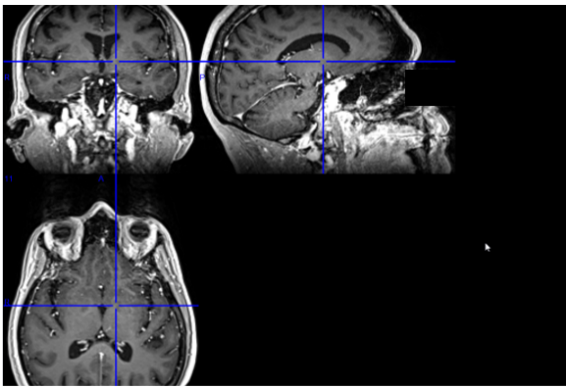

(a) Pre-operative MRI

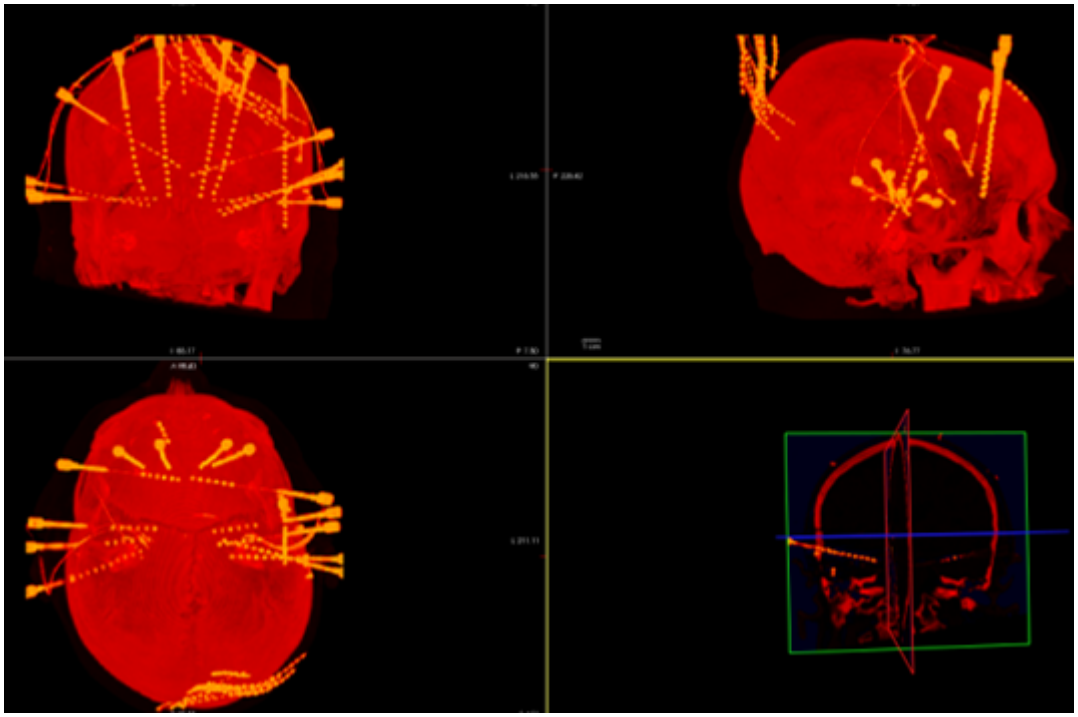

(b) Post-operative CT

Figure 2.2: Radiological Scans for a typical patient

these 2-D DICOM images are first combined to create a 3-D volume.

2. Freesurfer[25] is used to perform a set of processing stages called 'Reconstruction' on the three-dimensional MRI volume of the brain. A summary of the important steps is provided below-

a) Motion correction – Fixes any motion artifacts that might have crept in during the scan.

b) Intensity correction- Corrects for non-uniformity of intensity in the MRI data.

c) Normalization- performs intensity normalization to correct for fluctuations in intensity by scaling the intensity of all voxels to meet a pre-determined threshold.

d) Skull strip- removes the skull voxels from the MRI volume as the skull is not relevant to the anatomical localization.

e) Automatic subcortical segmentation- A multi-step process that involves initial registration to a template, neck removal, etc.

f) Normalization- post-skull removal normalization works better because the skull has a very high intensity.

g) White matter segmentation- Employs a combination of constraints pertaining to neighborhood, smoothness and intensity in order to separate the white matter from other the rest of the brain.

h) Neck removal- This step removes the neck from the rest of the head.

i) Labeling- The subcortical structures are labelled, followed by a computation of statistics for the patient.

j) Surface creation- Files are created for the left and right hemisphere pial surfaces.

k) Cortical parcellation- A neuroanatomical label is assigned to each location on the cortical surface. Lastly, statistics are computed for each structure.

Post-recon steps:

3. Visual inspection of recon output: Once Freesurfer completes reconstruction, the different output files are opened in the GUI to check for obvious defects and completeness of the

steps. Overlaying the parcellated atlas onto the T1-weighted MRI volume provides a good visualization of the various cortical as well as deep-brain structures.

4. We next load the original CT volume onto the MRI volume and transform it into the same coordinate space to achieve a good alignment. The transformed CT volume is then saved for further processing.

5. In the Interactive Electrode Localization Utility GUI, we set the path to the transformed CT volume as well as the reconstructed MRI folder. The coregistration process is then initiated.

The IELU algorithm[40] checks each voxel in the scan against a default intensity threshold, and the brightest point corresponds to an electrode contact point. In this way, each contact point is identified, and its RAS coordinates are obtained from the co-registered CT-MRI combination (see Fig. 2.3). The output is displayed on a 3D brain volume for the user to work on (see Fig. 2.8). Once all RAS coordinates are extracted from the pipeline, a custom MATLAB script is used to query the neuroanatomical atlas file of the patient, and the exact anatomical label for each RAS coordinate is determined. This gives us a lists of the exact regions where each contact point resides in (see Fig. 2.4). It is often noted that many points lie in regions like white matter, CSF, or bone. In that case it is of special interest to establish what nearest gray matter regions the given point might be picking up neural activity from (see Fig. 2.7). Therefore, we next create a table comprising of the nearest anatomical regions that each contact point's recording might be influenced by. In order to achieve this, we implement the step as described next.

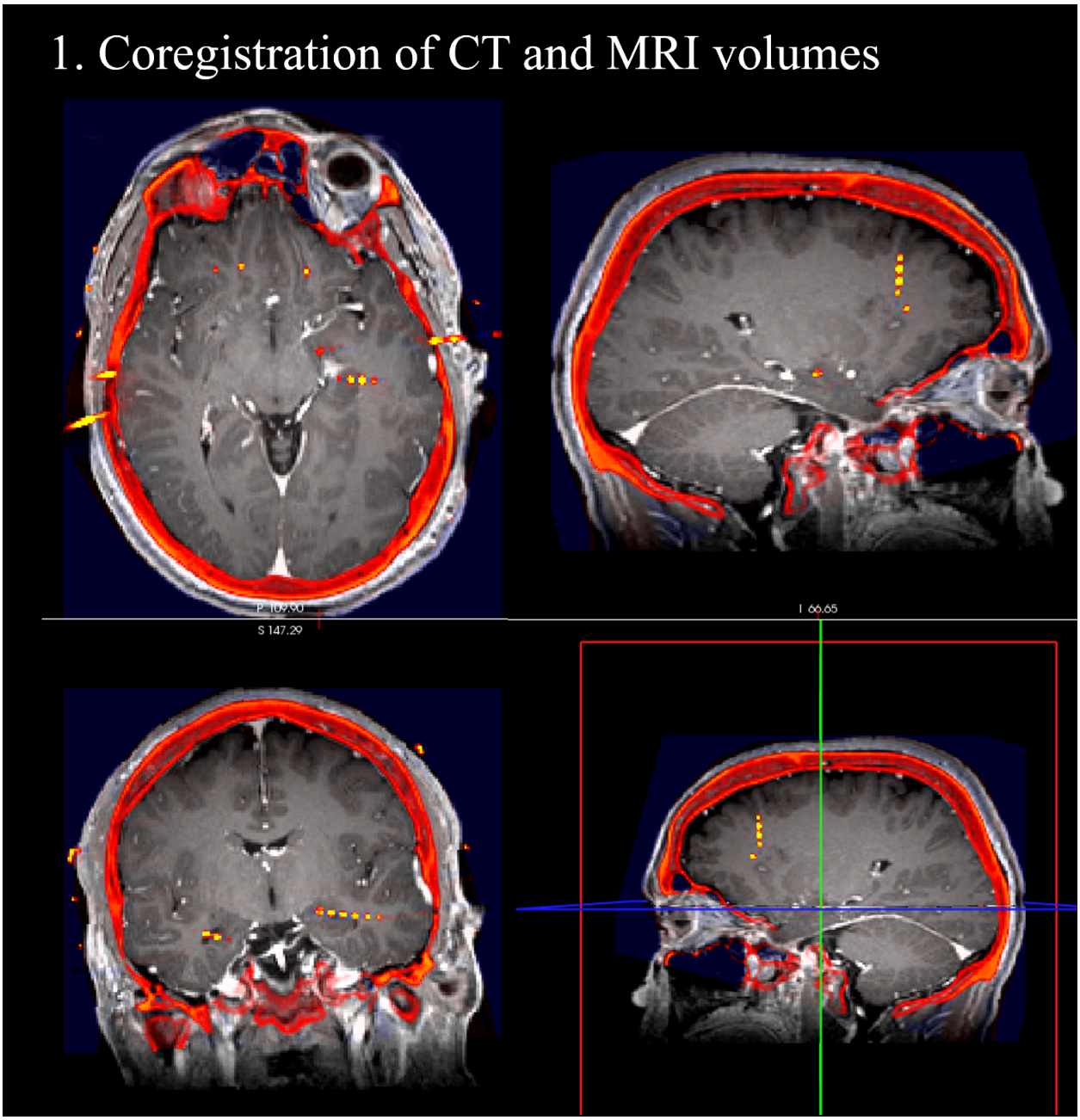

Figure 2.3: Coregistration output: A patient's CT overlayed on MRI.
Clockwise from top left – Axial, Sagittal and Coronal views

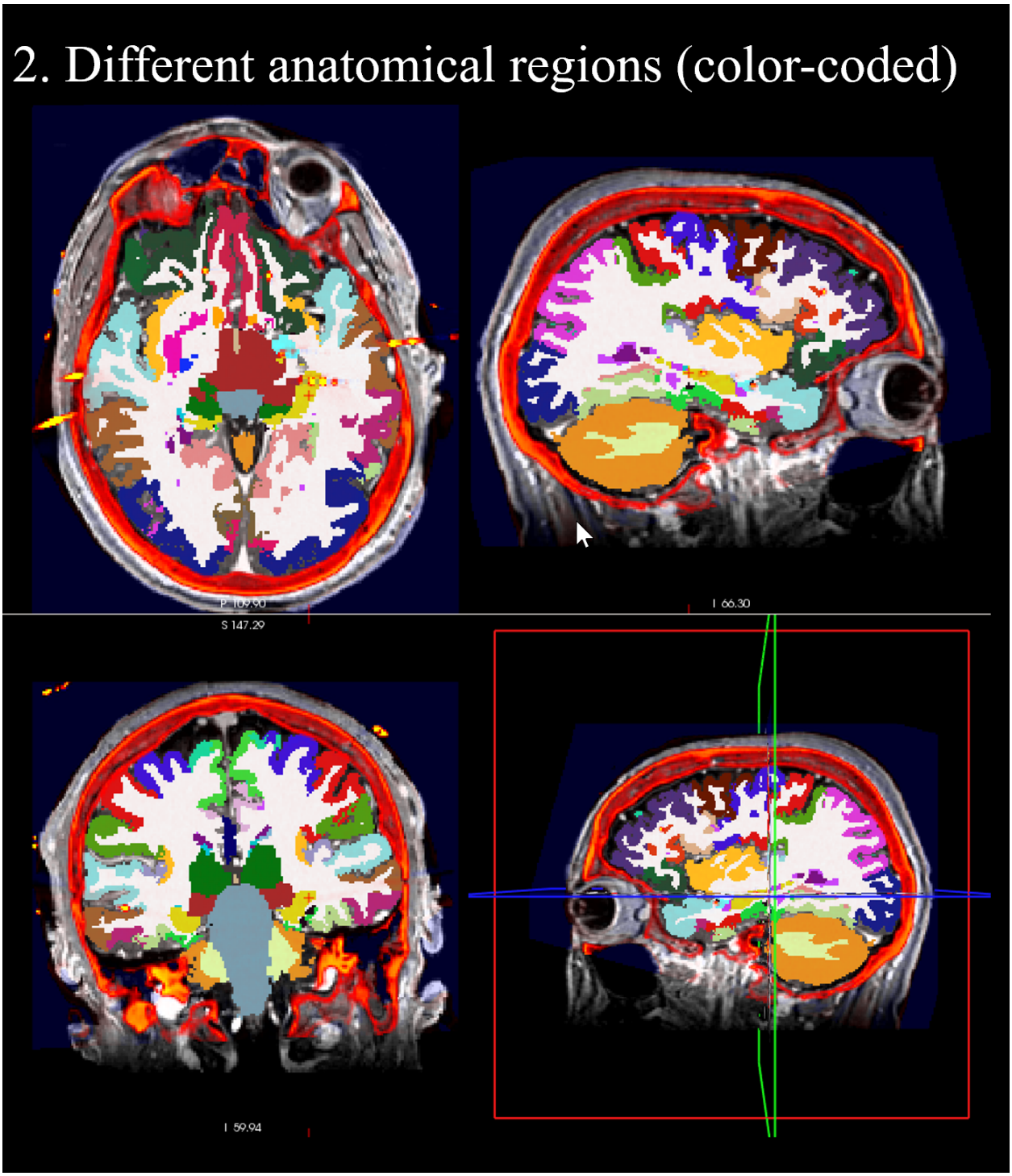

Figure 2.4: Color-coded Atlas map overlayed on the coregistration output.
Thalamus- Dark Green, Hippocampus- Light yellow, Mid temporal cortex – Brown, White matter - White

Figure 2.5: Q1. Where exactly is this electrode contact pt. residing? - Left Hippocampus

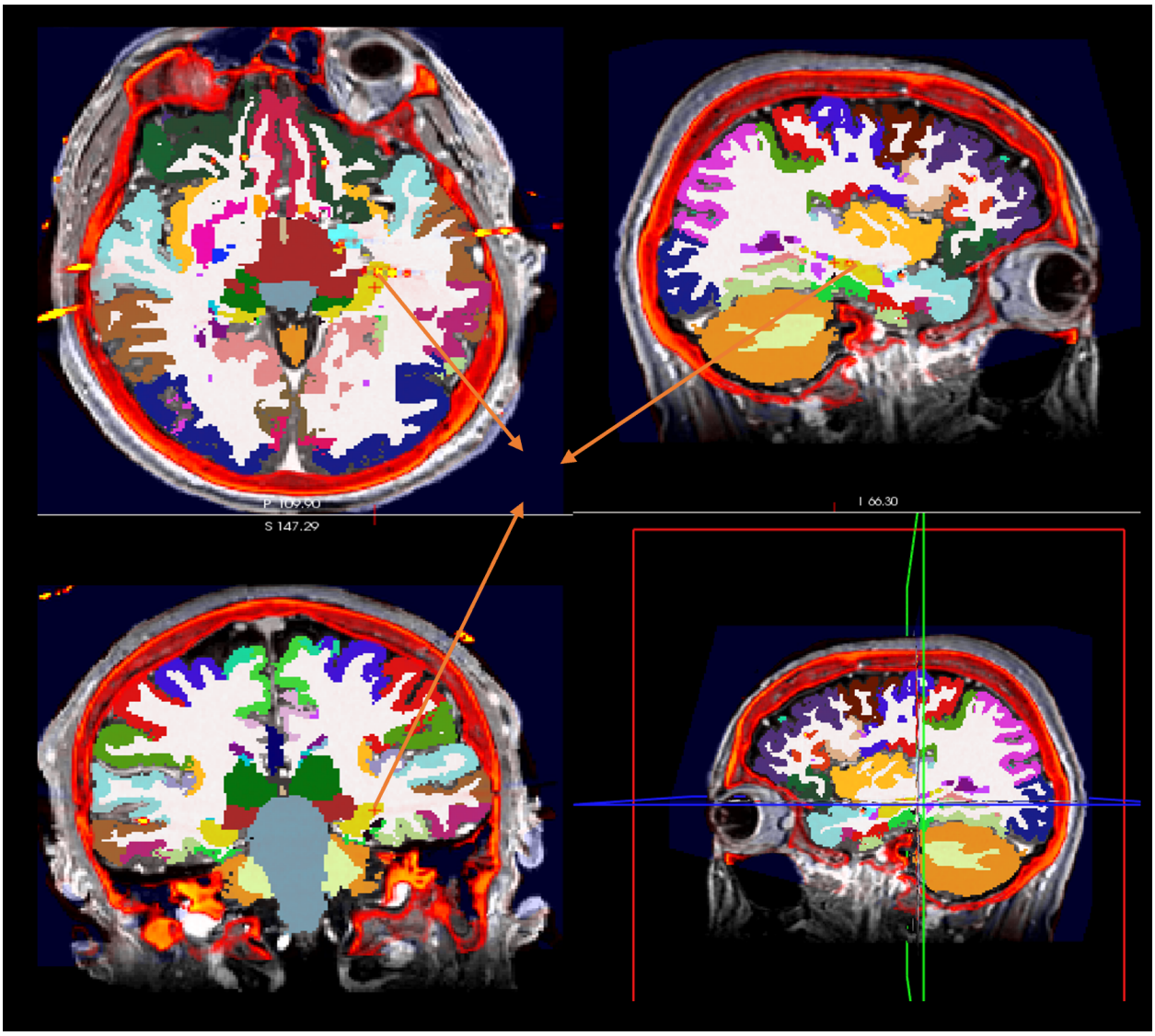

Figure 2.6: Different views of the same contact point located in the Left Hippocampus

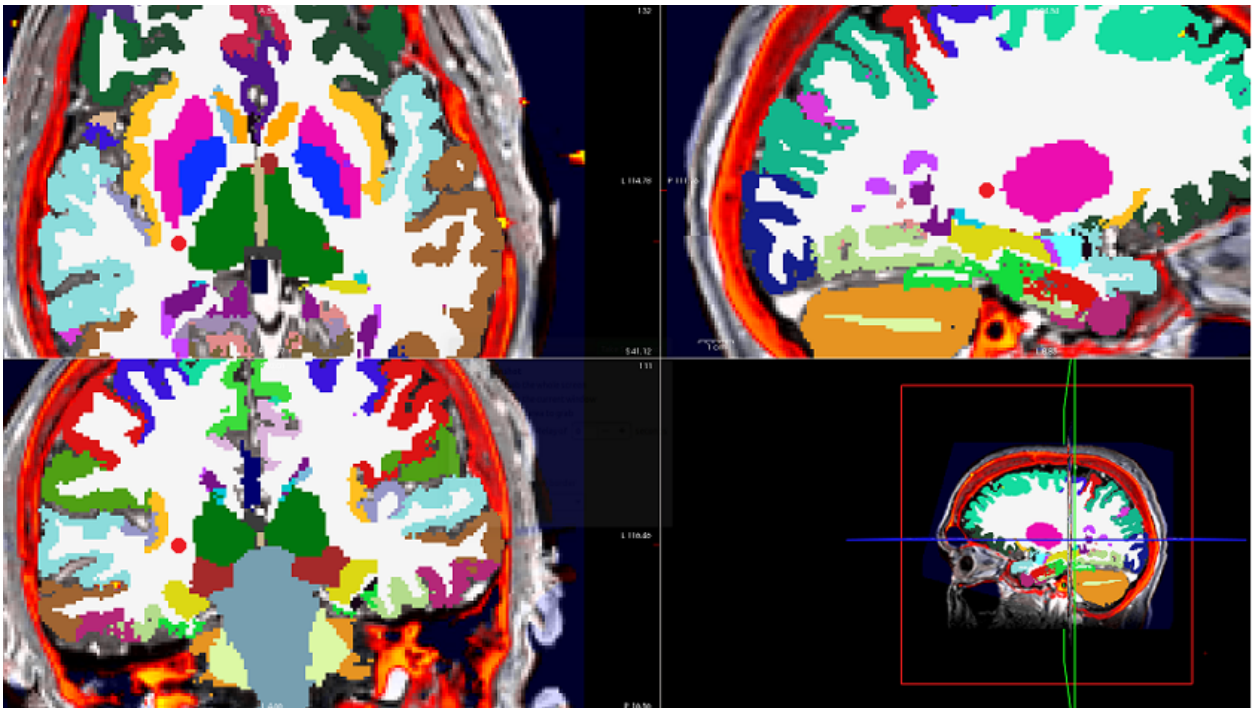

Figure 2.7: Q2. Nearest gray matter regions (to the contact point)?

2.3.1 Algorithm

An iterative inflation algorithm is implemented in MATLAB[31]. The RAS coordinates for a given contact point serve as the initial seed point. Around this point, a sphere of radius r is created. Next, coordinates of the points lying on this sphere are passed onto the next part of the algorithm, where we find the anatomical location of each generated point (see Fig. 2.9. We do this by querying the subject's ATLAS file generated during the reconstruction process. Thus, a list of the anatomical regions is created for a specific sphere, and the frequency of occurrence of each unique label is used to determine the order in which these regions contribute to the electrophysiological recordings obtained from that contact point. The value of the radius 'r' is then incremented, and the sphere generation process is repeated for this new value. Therefore, in successive iterations, increasingly larger spheres are generated around each contact point and the nearest anatomical locations are determined (see

Fig. 2.10. The increment size for the sphere radius, the distance between two generated points (resolution) and the limiting sphere size can be changed by the user.

Fig. 2.11 shows the localization results for nine electrode contact points for patient CAR 20.

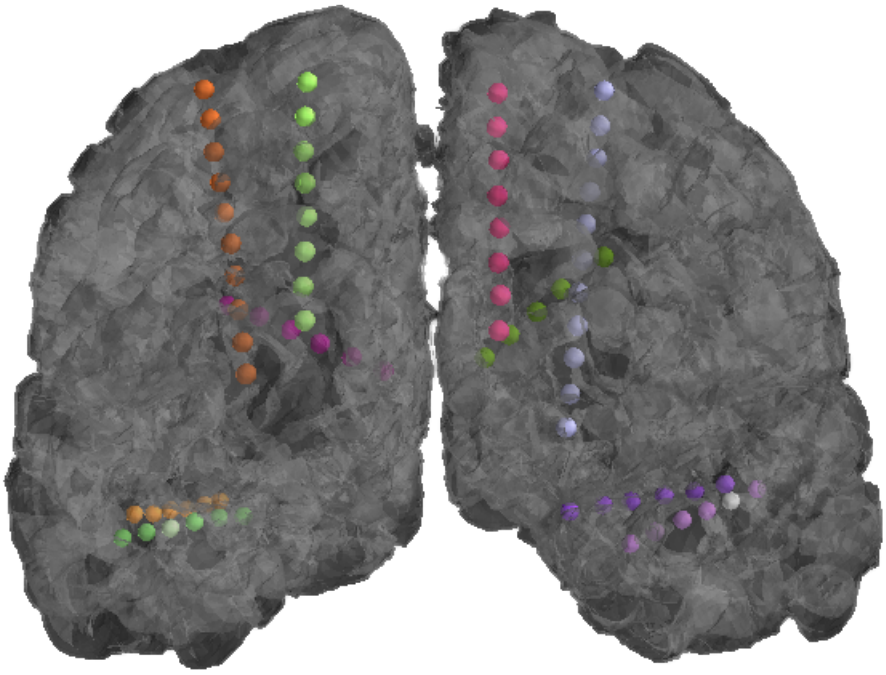

(a) IELU Output: Frontal View for Car 10 electrodes

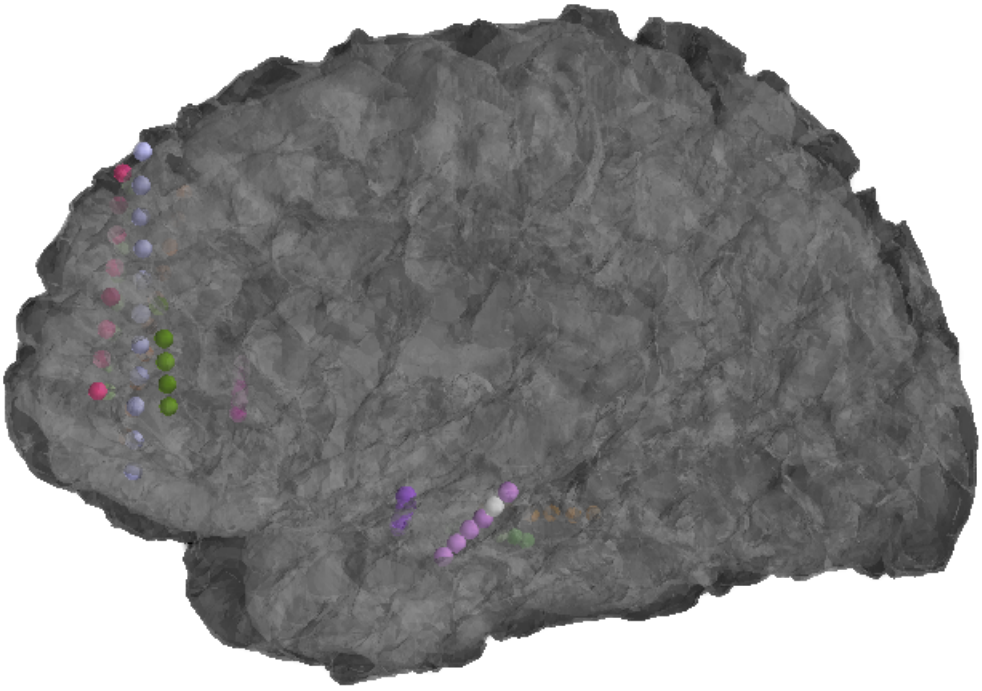

(b) IELU Output: Lateral View for Car 10 electrodes

Figure 2.8: Pipeline output for Electrode sets for patient CAR 10

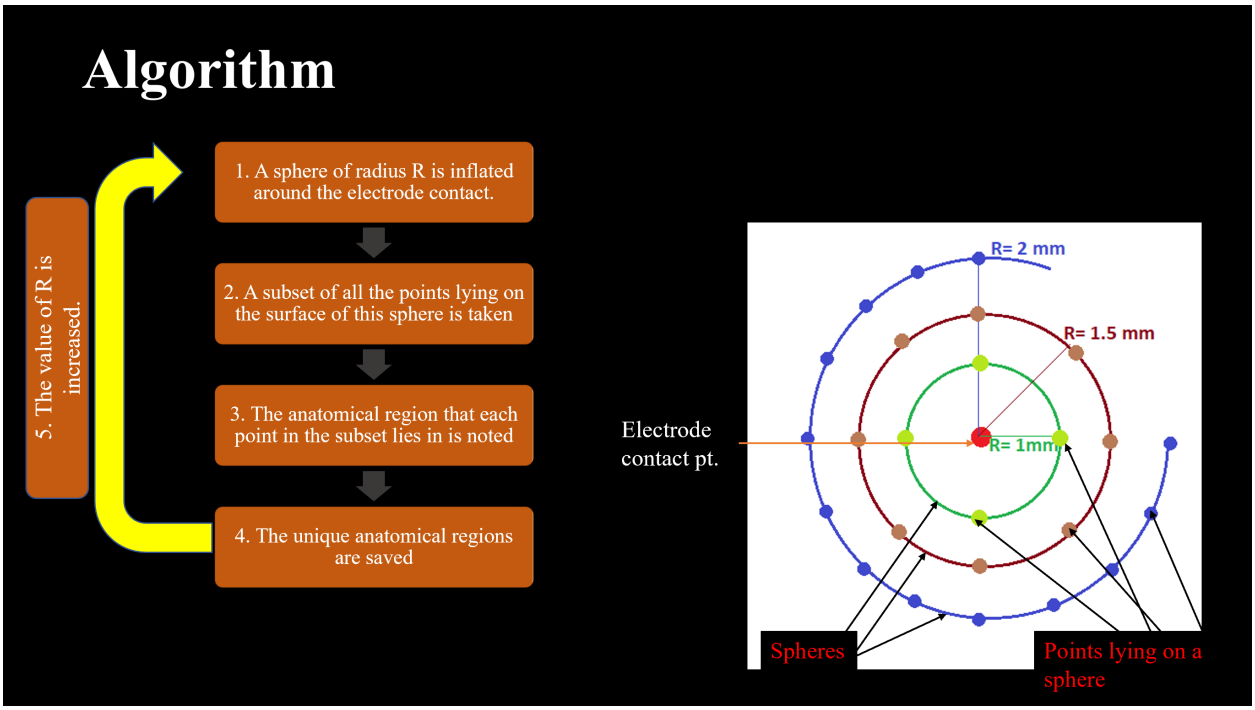

Figure 2.9: Algorithm: Sphere Inflation Method

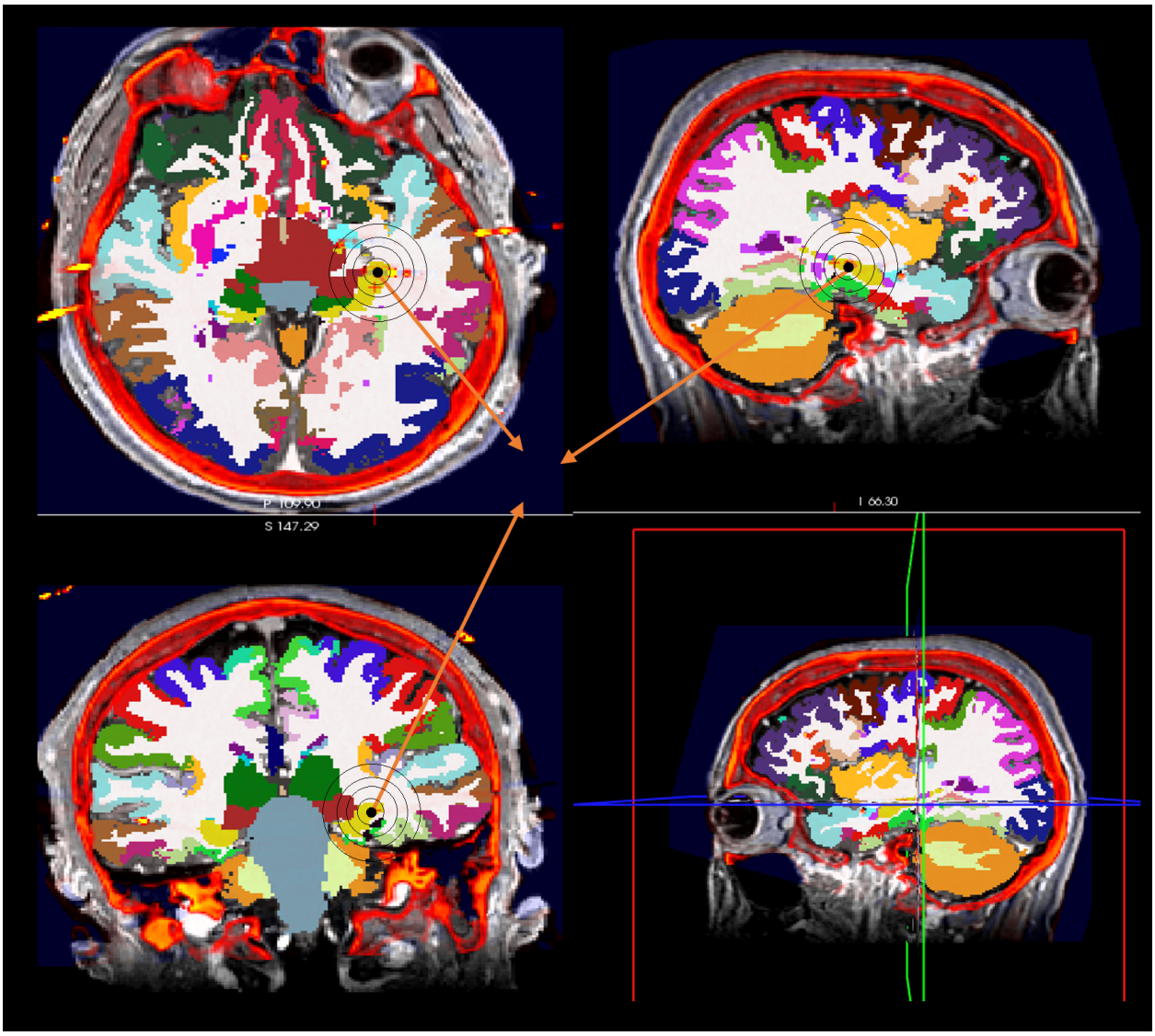

Figure 2.10: Spheres inflated around a contact point (shown in black)

Electrode Type	Medical Label	Coordinates (RAS)	Exact Location	Closest Region	2nd Closest Region	3rd Closest Region
Left Lateral to Amygdala	Amg-1Ld1	-17.53, 8.78, 0	Left-Amygdala	Left-Hippocampus	Unknown	ctx-lh-unknown
Left Lateral to Amygdala	Amg-1Ld4	-32.62, 8.52, -1	Left-Cerebral-White-Matter	Left-Amygdala	Left-Inf-Lat-Vent	ctx_lh_G_oc-temp_med-Parahip
Left Lateral Anterior to Hippocampus	AHipp-3Ld1	-17.66, 1.57, -2	Left-Hippocampus	Left-Cerebral-White-Matter	ctx-lh-unknown	ctx_lh_G_oc-temp_med-Parahip
Left Lateral Anterior to Hippocampus	AHipp-3Ld2	-22.61, 1.04, -1	Left-Hippocampus	Left-Cerebral-White-Matter	Left-Amygdala	ctx_lh_G_oc-temp_med-Parahip
Left Lateral Anterior to Hippocampus	AHipp-3Ld5	-38.01, 1.57, 0	Left-Cerebral-White-Matter	ctx_lh_S_collat_transv_ant	ctx_lh_S_temporal_sup	
Left Mid-Frontal to Orbital Gyrus	MFOG-11Ld4	-23.87, 61, 34.46	ctx_lh_S_front_middle	Left-Cerebral-White-Matter	ctx_lh_G_and_S_frontomargin	Unknown
Left Inferior-Frontal to Cingulate Gyrus	IFCG-13Ld1	-4.08, 44, 29.77	Left-Cerebral-White-Matter	ctx_lh_G_and_S_cingul-Ant	Unknown	ctx_lh_S_pericallosal
Right Lateral Posterior to Hippocampus	PHipp-8Rd1	26.1, -17.67, 8	Right-Hippocampus	Right-Cerebral-White-Matter	Unknown	Right-VentralDC
Right Lateral Posterior to Hippocampus	PHipp-8Rd3	36.35, -19.3, 8	Right-Cerebral-White-Matter	Right-Hippocampus	ctx_rh_S_temporal_sup	Unknown

Figure 2.11: Table: Exact and nearest anatomical locations for nine contact points in CAR 20

Chapter 3

Alpha Waves and Sleep

3.1 Introduction

Alpha waves are rhythmic oscillations of frequency 8-12 Hz. They are most prominent in the occipital regions and during eyes-closed wakefulness1.6). Numerous studies have been conducted to ascertain the exact nature and purpose of these waves in the mammalian brain[46, 59, 49, 14]. It is commonly believed that they are associated with lowered alertness and play a key role in inhibition or activation of different brain regions at different times[33]. For sleep scoring purposes, dominant alpha rhythm in the occipital region has been traditionally used to identify periods of wakefulness, and a decrease in its intensity indicates the subject's transitions to N1 sleep (light sleep).

Rapid Eye Movement Sleep (REM, 1.13) has some features that are similar to those found during wakefulness[45, 57, 9]. However, it is traditionally observed that the alpha power during REM drops noticeably compared to wakefulness in the occipital regions. Here, we investigated the behavior of alpha waves during different stages of sleep in the non-occipital brain regions as well, since a vast majority of intracranial EEG patients do not have electrodes in the occipital region. Specifically, we established the difference in alpha activity between Wake and REM stages in areas not confined to the occipital lobes.

3.2 Methods and Analyses

Six intracranial EEG patients undergoing monitoring for epilepsy were selected for these analyses. Selection criteria included at least one night of seizure-free sleep with verified REM and NREM sleep stages as well as non-faulty facial electrode recordings for manual sleep scoring. EEG activity was recorded using surgically implanted Ad-Tech electrodes[10]. For data analyses, we selected one or two outermost contact points from each electrode set provided they a) resided in a gray or white matter region closer to the cortex as determined by our electrode localization pipeline and b) did not pick up any interictal activity as reported by the epilepsy monitoring clinicians. Sleep EEG activity was continuously recorded overnight using the Neuralynx Pegasus system[44] with ATLAS on a Windows PC at 2KHz sampling frequency. Sleep data was visually inspected for artifacts and a subset of clean EEG channels was created. Sleep stages were identified for successive 30s epochs according to the standardized sleep scoring manual (AASM) [33]. Final sleep scores were compared, and REM periods were verified by three sleep scoring experts.

3.2.1 Overnight Hilbert power

EEG data from the selected montage of channels was passed through a 60 Hz notch filter to get rid of power line interference. The data was mean subtracted to remove the DC offset caused by recording equipment and drift. This data was then passed through an FIR Bandpass Filter (8-12Hz) to extract alpha activity[11]. The Hilbert transform [35] for each channel was computed and the real part was extracted to obtain the Hilbert envelope. This envelope served as an accurate representation of the true electrical power. The alpha power variation for each individual channel as well as the average of all channels was plotted against the hypnogram for the entire night.

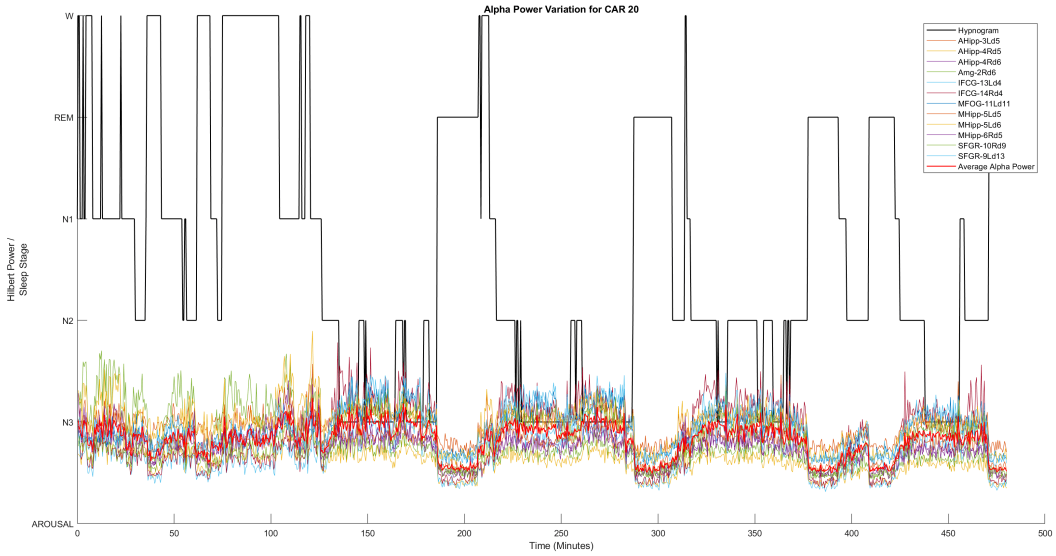

(a) Alpha Power Variation for Individual Channels.

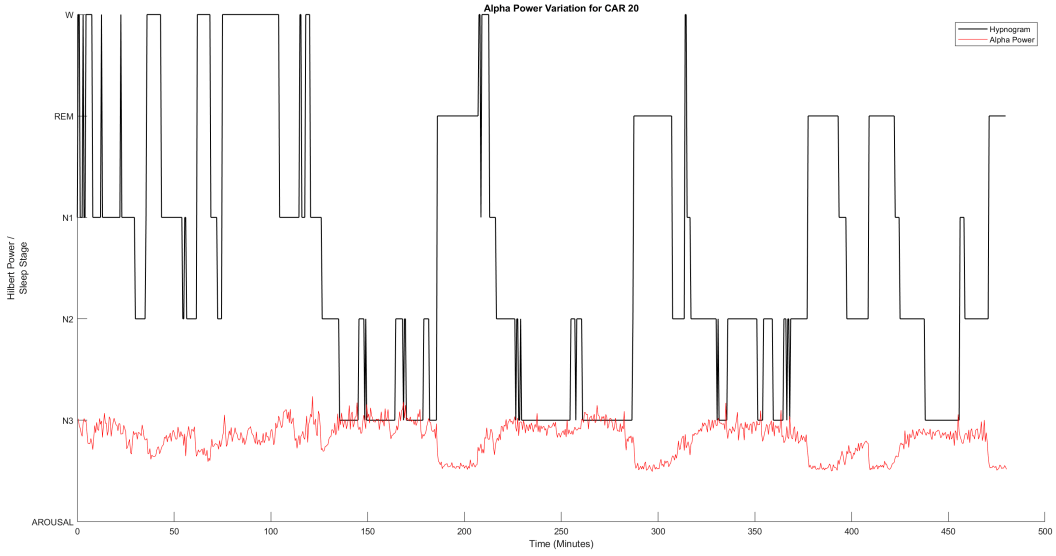

(b) Alpha Power Variation across Channels.

Figure 3.1: Alpha Power and Hypnogram for CAR 20

Fig. 3.1 shows that the alpha power drops below its baseline level/value around each REM period. Specifically, the alpha power remains lower during REM in comparison to Wake and N1 periods.

3.2.2 Hilbert Power Relationships

Six intracranial subjects were considered for the following analysis. For each subject, one full night of seizure-free and REM-inclusive sleep was manually scored and compared by three experts. Facial electrodes (EOG and EMG) were also consulted to determine the different sleep stages (categorized as 30-second epochs). The AASM standard was used as the scoring reference. The Neuralynx Pegasus system was used to record the EEG signals at 2KHz. For each subject, recordings from a set of electrodes were first mean subtracted to get rid of DC offset, then passed through a 60Hz notch filter to filter out power line interference. Next, each channel was band-passed between 8 – 12 Hz using EEGLAB[18] in MATLAB with zero phase shift. The Hilbert envelope was then computed, and the absolute part was taken to be an approximation for the Hilbert power present in each channel. The average power was calculated for each 30s epoch, and two sets were created for W and REM stages.

Statistical test: A two-sampled, unpaired t-test was performed assuming unequal variances between the W and REM power values. The channels that were investigated were all clean and non-interictal[13], close to the cortical surface, and lied in gray matter regions. At 95% confidence interval, each channel for each patient showed that alpha power during Wake was significantly higher than that during REM. Next, the Hilbert power was log transformed, and t-tests revealed significant difference (with W>REM) between W and REM periods. A thousand shuffles were implemented to create surrogate sets comprising of equal number of W and REM power values, and t-tests were performed on these surrogates as well. It was observed that the p-value for the original W vs. REM t-test was still significantly smaller

than those for the surrogate tests. To further check for robustness, an equal number of W and REM values (n= 30% of the lower no. of epochs between W and REM) were randomly selected without replacement from the parent sets, and the t-tests were repeated. The t-tests again yielded significant difference (W > REM) for all channels and subjects. Therefore, it was determined that alpha power during W was significantly higher than that during REM in these subjects (see Fig. 3.2).

3.2.3 Exploration of other Relationships

We looked at a number of other temporal relationships. Among these, one possibility we considered was cross-coherence relationships[19, 57] between W and REM. To investigate this, a bipolar montage was implemented to reference the channel data i.e., successive channels were paired, and the resultant data was obtained by taking the difference between the two channels in each pair. This re-referenced data was then divided into 2-second periods and each period was mean subtracted to remove its DC drift. The coherence between pairs of re-referenced channels was computed during Wake, REM and entire night. A theoretical confidence level was obtained to determine significance of high coherence periods. No consistent relationships found across the subjects. For example, in 3.3, CAR 20 showed significant relationship between channels AHipp5 and Amg5, but not for other pairs. CAR 16, on the other hand, showed strong coherence in the alpha band for two channel pairs. These inconsistencies may be due to patient variability or other unaccounted for factors, and might be a topic for future exploration.

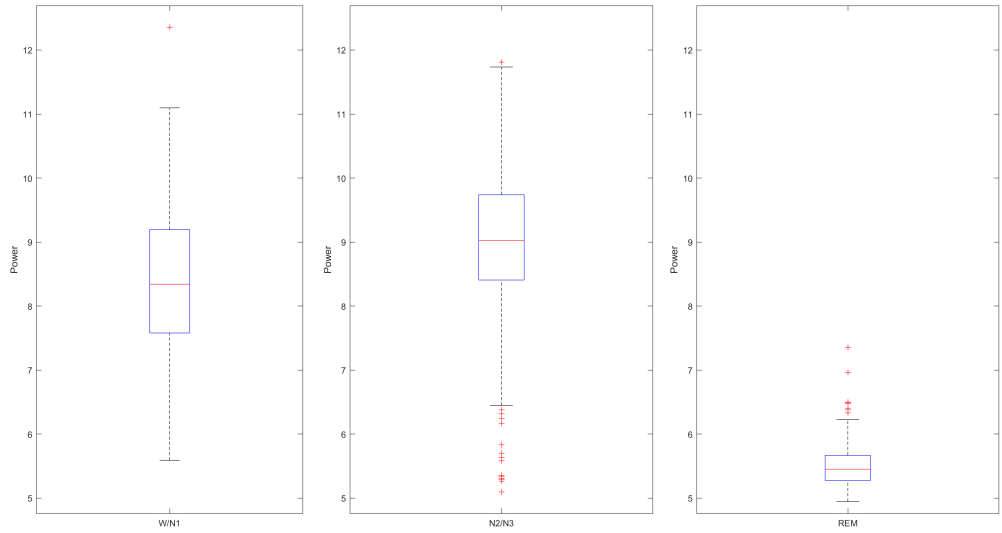

(a) Alpha Power Distribution across Sleep Stages for CAR 20.

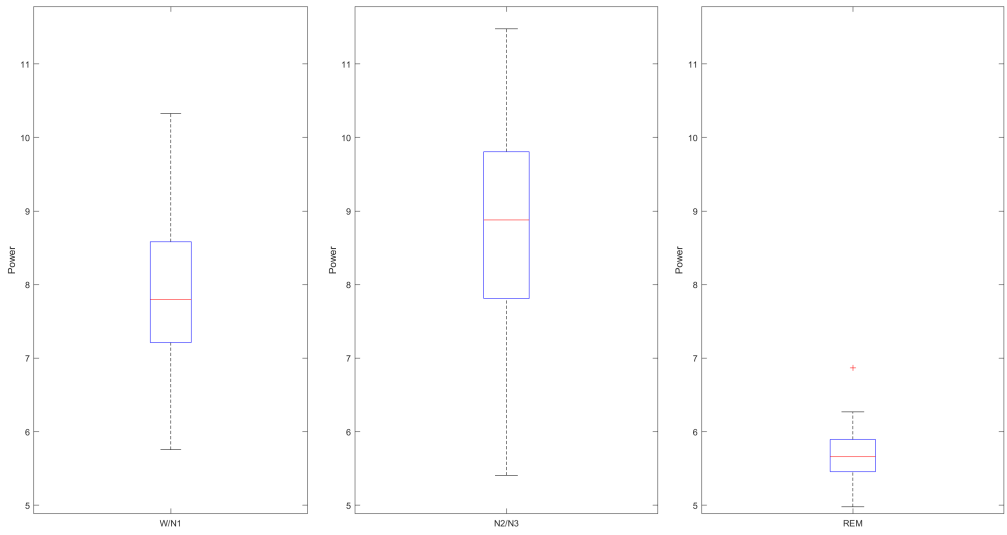

(b) Alpha Power Distribution across Sleep Stages for CAR 16.

Figure 3.2: Alpha Power Box and Whisker Plots

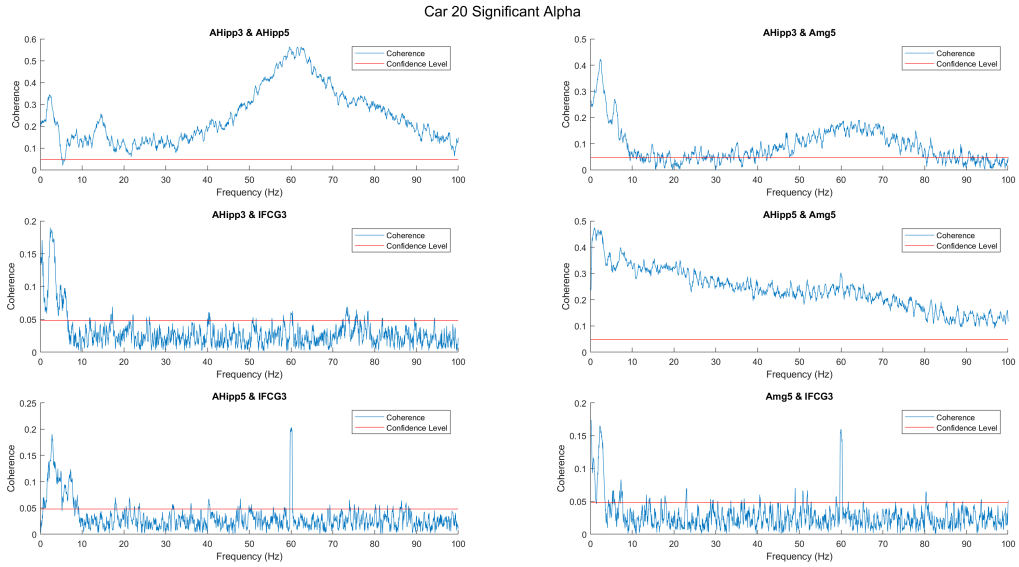

(a) Cross-coherence among Four channels for CAR 20.

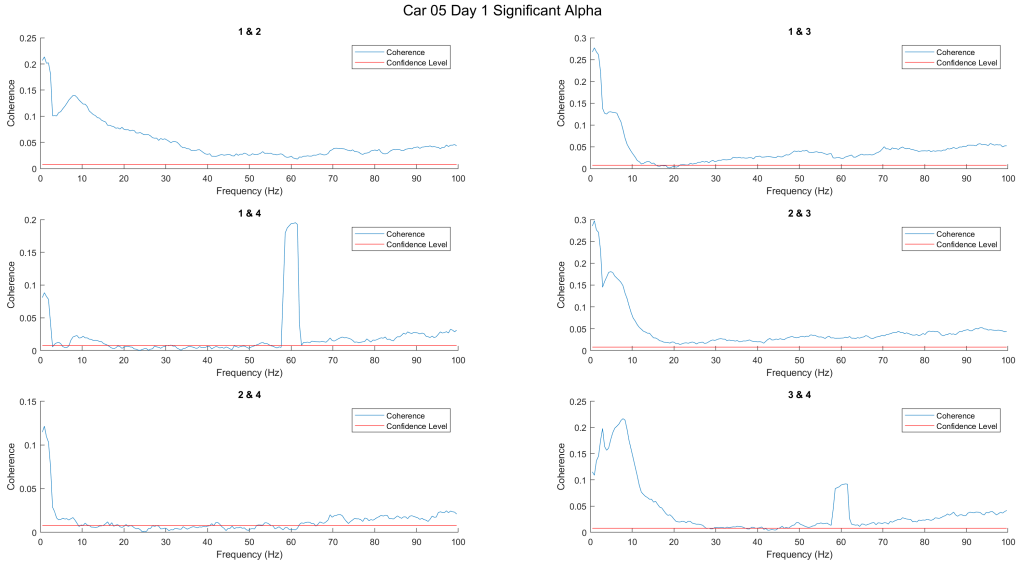

(b) Cross-coherence among Four channels for CAR 16.

Figure 3.3: Cross-Coherence Plots for four hours of sleep

3.2.4 Fitting Binormal Distributions

Alpha power was found to be lower during REM than during Wake and other stages. To quantify the difference and establish the threshold level to distinguish between Wake and REM alpha power, a number of methods were implemented before establishing a Gaussian mixture model[48] fit method. Assuming that the alpha power values for Wake and REM form a mixture of two bivariate Gaussian distributions, a k-means clustering algorithm[42] was implemented in MATLAB to fit two normal distributions to the data (see Fig. 3.4). It was found that the distributions were a better fit when all sleep stages were included as opposed to only Wake and REM (since REM alpha power is significantly lower than other sleep and wake stages, it is fair to assume that the alpha power distribution throughout the night comprises of a) a normal distribution containing REM alpha power whose mean is significantly lesser b) a normal distribution containing alpha power from W, N1, N2 and N3 stages since these stages seem to have comparable levels of alpha power. Increasing the sample size by including other sleep stages aids in fitting a better model to the data, thereby providing a better threshold value). The threshold obtained from the fit proved to be a good parameter in the automated sleep scoring steps as described later. Visual inspection of figure 1 provides further support in favour of the automated threshold obtained from this step. Additionally, histograms depicting the alpha power values for individual channels as well as the average alpha power across channels also highlight the bimodal nature of the data.

3.2.5 Automated Scoring (Wake vs. REM)

For the purpose of automatically distinguishing between Wake and REM epochs, the alpha threshold value was determined using the Binormal Fitting method [42, 43] as described in

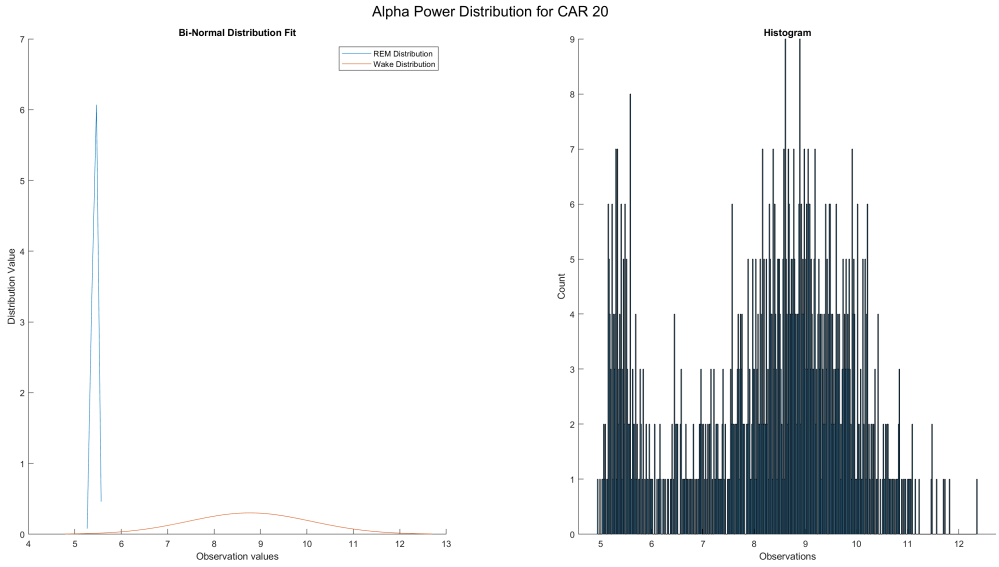

(a) Distribution Fit for all Alpha Power

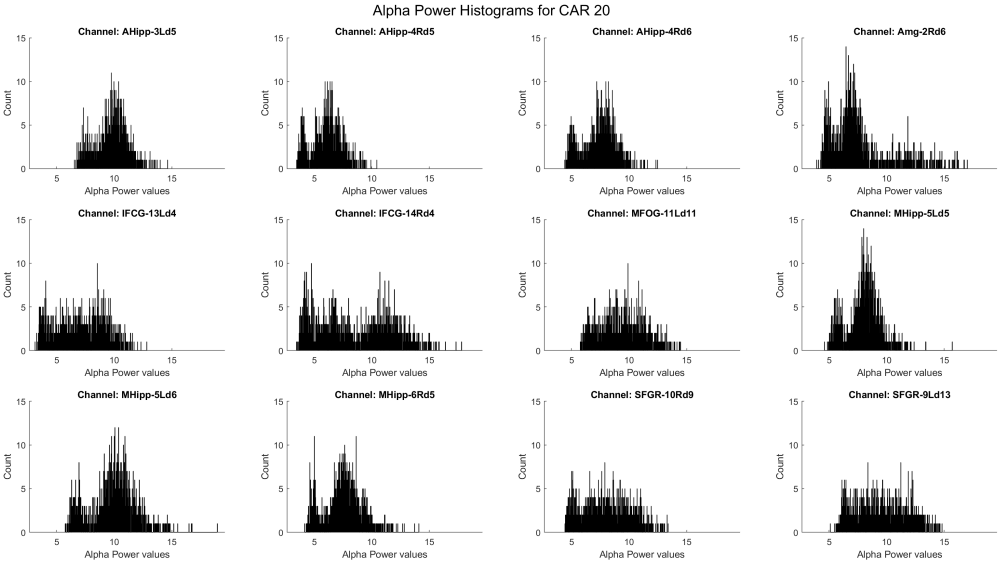

(b) Histograms for Individual Channels for all Alpha Power

Figure 3.4: Fitting Two Normal Distributions to Alpha Power

section 3.2.4 above. The manual sleep score was consulted to extract only the Wake and REM periods. The average alpha Hilbert power for each of these epochs comprised of the initial data set. By using the k-means clustering algorithm, two normal distributions were fitted to this data and the (mean + standard deviation) value was chosen as the threshold between Wake and REM. therefore, epochs having alpha power lower than this threshold were classified as REM whereas the remaining epochs were classified as W/N1. Based on this method, we were able to separate REM from Wake / N1 with good accuracy. A detailed summary of the classification accuracy for each subjects is shown below (Table 3.1):

Table 3.1: Automated Wake-REM Classification using Alpha Power

Subject	Total No. of Epochs	Accuracy(%)
Car 04	589	91.34
Car 05	141	92.34
Car 06	315	88.57
Car 12	676	81.95
Car 16	77	95.36
Car 20	158	96.70

Chapter 4

Automated Sleep Scoring

4.1 Introduction

Sleep scoring is a method that employs a set of rules to classify a subject's sleep into five different stages- Wake (W), Non-REM 1 (N1), Non-REM 2 (N2), Non-REM 3 (N3), and Rapid Eye Movement (REM) (Section 1.4). Traditionally, a human sleep scoring expert visually inspects EEG activity from different regions of the brain along with electromyogram (EMG, chin muscle tone) and electrooculogram (EOG, or eye muscle movement) to classify successive 30-second time periods called epochs into one of the five stages. The expert determines the sleep stages based on various stage-specific as well as generalized features like different brain waves, neural signatures, muscle tone and eye movements (see Fig. 1.9, 1.10, 1.12, 1.13). For example, in a typical subject W is associated with dominant alpha wave rhythm (8 -12 Hz) in the occipital regions, N2 is associated with K-complexes[1] and sleep spindles (sigma waves, 12-16 Hz), N3 features large amplitude delta waves, and REM is accompanied by rapid eye movements combined with low muscle tone. Conventional sleep scoring relies heavily on the facial electrodes (EMG and EOG) to distinguish W from other stages, and to identify arousals as well as REM. It also depends on the specific sleep scorer's discretion and judgement[17, 60] especially for epochs that are tricky to assign one of say two stages.

While dedicated sleep studies (clinical or research-based) are extremely likely to include

facial electrodes in their montage, most intracranial EEG recordings at thousands of sites across the world are not accompanied by these supplementary recordings. This is mainly due to the fact that patients suffering from drug-resistant epilepsy and other disorders form the largest percentage of this data pool, and they undergo invasive EEG monitoring to localize an epileptic focus or other damaged tissue in their brain for future resection. Therefore, sleep scoring remains irrelevant to their clinical diagnosis and their electrophysiological monitoring is limited to intracranial and scalp recording sites only.

In order to tap into this vast pool of brain activity recordings, and to investigate neural dynamics present during sleep it is crucial to first implement a sleep scoring method that can be used on these recordings where facial electrodes are absent i.e., to be able to accurately classify the subjects' sleep based solely on their EEG activity without the aid of muscle tone or eye movement data. Specifically, since many learning and memory processes are believed to depend on NREM sleep (N2 and N3) as well as REM sleep, it is of special interest to come up with a reliable method to separate the REM and N2/N3 periods from the rest of the data. In this chapter we present an automated method to classify epochs into W/N1, N2/N3, and REM sleep stages with the use of Delta wave and Alpha wave activity present throughout the entire duration of sleep.

As discussed in Chapter 3 (specifically sections 3.2.4 and 3.2.5), we have already established a reliable metric for REM vs. W/N1 classification provided that the initial data belongs to only the W/N1 and REM epochs. We used a binormal distribution fit to determine the alpha power threshold that separates the REM epochs from W and N1 (see Fig. 3.4). In fact, this method is extremely reliable in identifying the REM periods regardless of the inclusion of N2 and N3 data along with W and N1 (Table 4.1). Therefore, we can successfully identify REM periods during sleep using the alpha power variability (REM was always found to have the lowest alpha power among all stages). However, in order to implement a more robust and complete sleep scoring method we need to first separate the N2 and N3 epochs from the

remaining data, after which we can execute this step.

Delta waves (0-4Hz, >75uV amplitude, see Fig. 1.12) are one of the main features of N3 and even N2 sleep. While a typical subject's N2 sleep is dominated more by sleep spindles (12-16Hz, see Fig. 1.11), a gradual build-up of delta waves is often observed in this stage which ultimately transitions into N3 sleep. This delta wave activity is found to be significantly low during W, N1 and REM stages (see Fig. 4.2, 4.3). Thus, by using delta power variation as a representation of delta activity during sleep, we established a method to identify periods of N2 and N3 sleep in our data.

4.2 Method

From six subjects' raw EEG data, a subset of channels was chosen as per the criteria mentioned in Ch. 3. The data was passed through a 60 Hz notch filter to remove power line interference, followed by mean subtraction to get rid of the D.C. drift. For the delta power analysis, this data was passed through a band-pass filter in the delta wave range (0-4Hz). From the filtered data, the Hilbert envelope was computed; the real part of this envelope served as a good approximation for the instantaneous Hilbert power associated with each channel under consideration. The average power was calculated across all channels. Next, for each 30s epoch, the average Hilbert power was computed such that each epoch was represented by one average delta power value. The entire process was repeated to calculate the average alpha power value per epoch. Thus, for each subject, there was a set of delta power as well as alpha power values. The duration of continuous sleep/wake recordings for each subject was around 480 to 720 minutes (one night).

For automated scoring purpose, W and N1 were assumed to be a single stage representing wakefulness, N2 and N3 were combined to represent Non-REM sleep, and REM was treated

as a separate stage.

Step 1: Separating N2/N3 stages from W/N1 and R- A binormal fit was applied to the resultant average delta power data set. The (mean + standard deviation) parameter was used to determine a threshold above which the epochs were classified as N2/N3.

Step 2: Separating R from W/N1- A binormal fit was applied to the average alpha power set to determine the alpha power threshold below which the epochs were classified as REM.

Algorithm: Assuming a1 be the alpha threshold, d1 be the delta threshold,

if Delta > d1 => Epoch is N2/N3

else, if Alpha>a1 => Epoch is Wake

else => Epoch is REM

4.3 Results

The following results were obtained for the six subjects:

Table 4.1: Automated Sleep Scoring Results

Subject	Initial Accuracy(%)	Final Accuracy(%)
Car 04	42	62
Car 05	57	83
Car 06	40	60
Car 12	53	87
Car 16	83	83
Car 20	87	87

The column 'Initial Accuracy' refers to the accuracy achieved when we strictly used the (mean + 1 standard deviation) threshold estimated from the binormal distribution fit. In some patients, due to large differences in the delta power amplitude during NREM as opposed to other stages, as well as temporal variability, the above mentioned threshold may not be

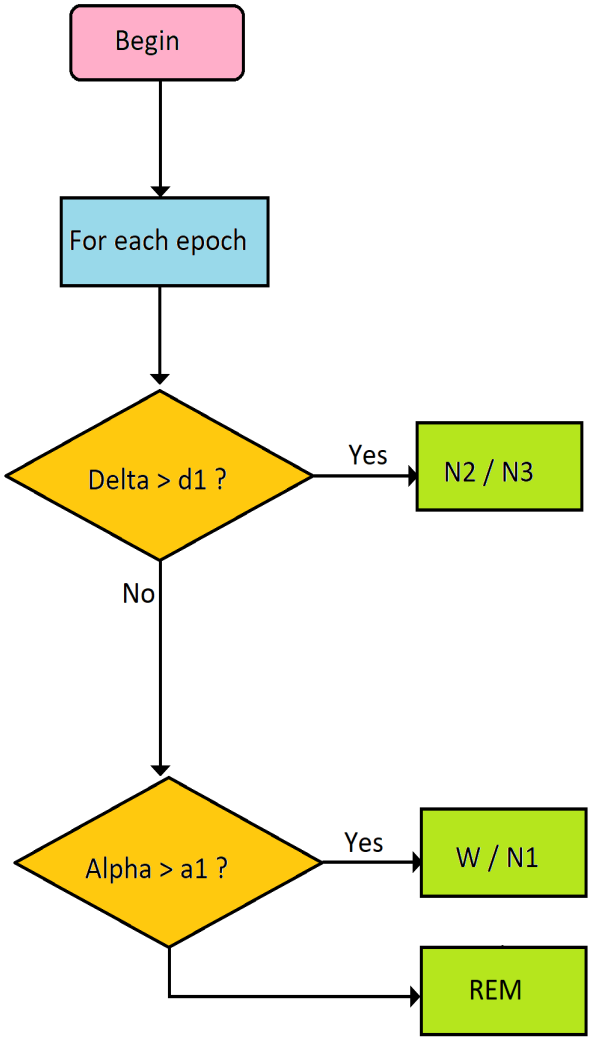

Figure 4.1: Flowchart

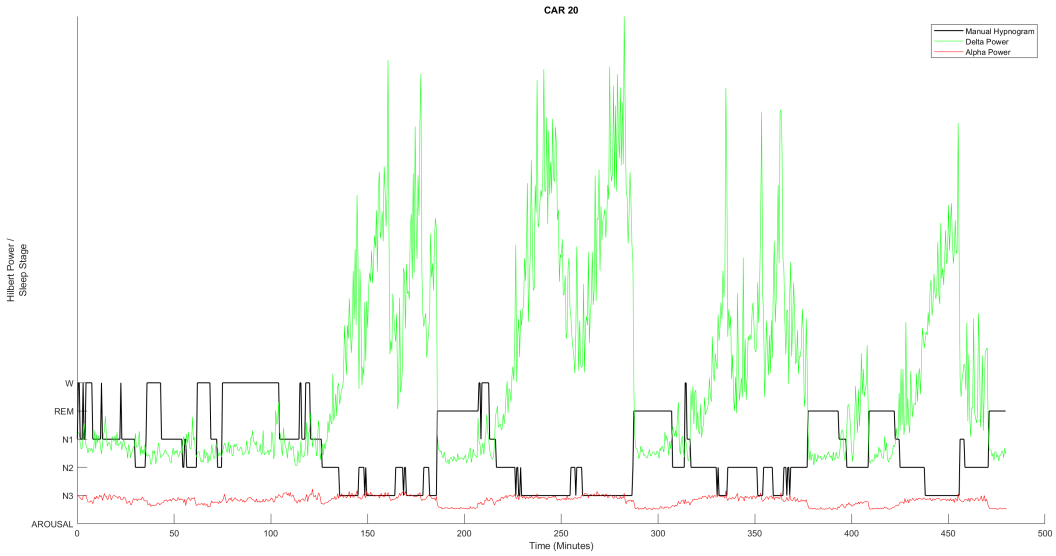

Figure 4.2: CAR 20 Power Variation

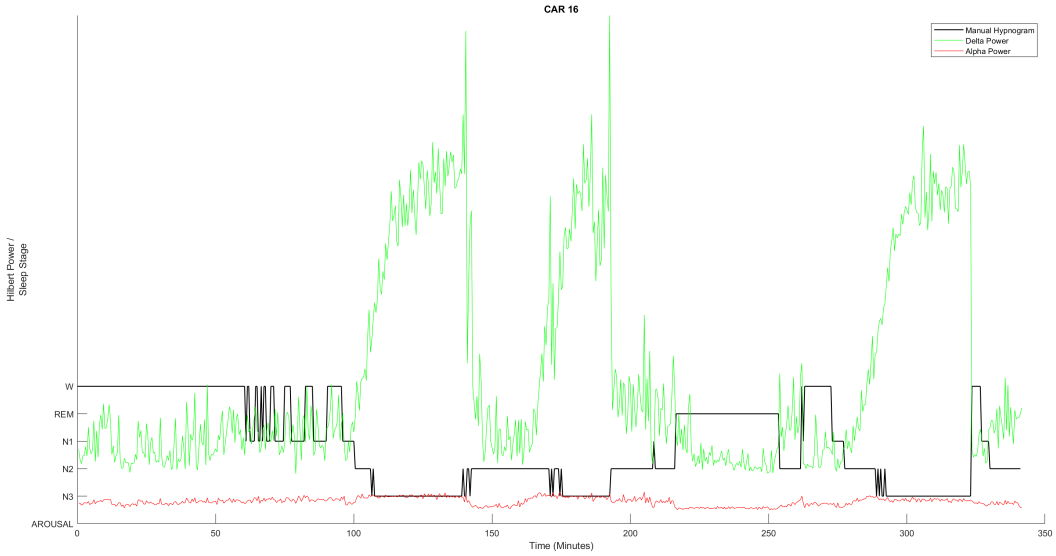

Figure 4.3: CAR 16 Power Variation

high enough to separate W, N1 and REM from N2 and N3 stages. In this case, a feasibility check was implemented by checking the delta power variation over time, as shown in Fig. 3.1. By visually inspecting the highs and lows in the delta wave variation, it is possible to determine whether the threshold (mean + 2 Standard deviations) might be a much better threshold. Therefore, for patients whose initial accuracy levels were low (i.e., CAR 04, CAR 05, CAR 06, CAR 12) we used the revised threshold and achieved the final accuracy levels as shown in Table 4.1. Additionally, the following relationships were observed among the sleep stages with respect to alpha power (Table 4.2):

Table 4.2: Alpha Power Relationship among Sleep Stages

Subject	Relationship
Car 04	N3>W>R
Car 05	W>N3>R
Car 06	N3>W>R
Car 12	N3>W>R
Car 16	W=N3>R
Car 20	N3>W>R

A few challenges encountered while implementing this automated scoring algorithm were related to actually picking the threshold, uncertainties over manually scoring N1 epochs, dealing with noisy channels, and accounting for the patients' irregular sleeping patterns. Fine-tuning the threshold estimation step will be a topic for future exploration.

Chapter 5

Conclusions

The overarching goal of our work has been to render thousands of electrophysiology data sets lying across the world useful for sleep studies and investigation of neural dynamics governing memory and learning.

We first designed and verified a method to reliably label the true sources of electrophysiological activity that is recorded by each individual electrode contact point in iEEG patients. While the clinicians have an approximate idea of where the electrodes will be placed, factors like post-operative inflammation, bleeding, tissue resistance encountered while guiding the electrodes during implantation, and shift in the brain matter all cause the electrodes to undergo some degree of deviation from their intended trajectories. Furthermore, for diagnostic purposes, it is sufficient for the clinician to determine a coarser region that a given recording site is picking up activity from. On the other hand, to use these recordings for research purposes it is of utmost importance that the channel data can be attributed to highly localized as well as properly delineated anatomical regions that might serve specific functions. Driven by this need, we started off by locating each recording site in the three-dimensional space with a level of precision that exceeds the clinical requirement. We then developed an iterative inflation algorithm that determined a list of functionally relevant gray matter regions that any given recording site could be picking up activity from, as well as estimate the degree of influence based on proximity to the said recording site. We successfully implemented the localization method for over fifteen intracranial EEG patients.

Having established the anatomical locations for our channels, we then proceeded to solve the problem of scoring these data sets that lacked recordings from occipital regions, as well as EOG and EMG electrodes. Traditionally, alpha power has been used from the occipital regions of the brain with the help of Electrooculogram and Electromyogram recordings to distinguish between W and REM stages during sleep. This has also been primarily implemented for conventional EEG subjects with a complete electrode setup (10-20 system) in dedicated sleep labs aided with the help of EOG and EMG electrodes. However, as far as intracranial EEG studies and clinical data are concerned, most patients do not have recording sites in the occipital regions to begin with, since the temporal and frontal lobe regions are more relevant to the clinical objectives for invasive EEG monitoring. Therefore, we first aimed to establish that there is a significant difference in alpha wave activity between Wake and REM stages which extends beyond the occipital regions in these patients. Upon successful demonstration of the said difference, we introduced an automated method to classify the sleep data into sleep stages on the basis of variation in the alpha and delta bands power during sleep. Specifically, we were able to identify REM periods during sleep strictly without the aid of EOG and EMG recordings. By doing so, we have made it possible for researchers to meaningfully use the vast collection of sleep data that has been relatively untapped so far, in hospitals and labs across the world for sleep-related analyses. We hope that our work can better ascertain electrode locations, sleep staging and therefore aid the community of labs studying sleep related dynamics worldwide.

Bibliography

[1] Florin Amzica and Mircea Steriade. "The functional significance of K-complexes". In: *Sleep medicine reviews* 6.2 (2002), pp. 139–149.

[2] Eishi Asano et al. "Origin and propagation of epileptic spasms delineated on electrocorticography". In: *Epilepsia* 46.7 (2005), pp. 1086–1097.

[3] Issam A Awad et al. "Intractable epilepsy and structural lesions of the brain: mapping, resection strategies, and seizure outcome". In: *Epilepsia* 32.2 (1991), pp. 179–186.

[4] Bengi Baran et al. "Processing of emotional reactivity and emotional memory over sleep". In: *Journal of Neuroscience* 32.3 (2012), pp. 1035–1042.

[5] Sarice Bassin, Teresa L Smith, and Thomas P Bleck. "Clinical review: status epilepticus". In: *Critical Care* 6.2 (2002), pp. 1–6.

[6] Leonardo Bonilha et al. "Medial temporal lobe epilepsy is associated with neuronal fibre loss and paradoxical increase in structural connectivity of limbic structures". In: *Journal of Neurology, Neurosurgery & Psychiatry* 83.9 (2012), pp. 903–909.

[7] Paul Boon et al. "Deep brain stimulation in patients with refractory temporal lobe epilepsy". In: *Epilepsia* 48.8 (2007), pp. 1551–1560.

[8] Thorsten M Buzug. "Computed tomography". In: *Springer handbook of medical technology*. Springer, 2011, pp. 311–342.

[9] JM Calvo and Augusto Fernández-Guardiola. "Phasic activity of the basolateral amygdala, cingulate gyrus, and hippocampus during REM sleep in the cat". In: *Sleep* 7.3 (1984), pp. 202–210.

[10] David W Carmichael et al. “Safety of localizing epilepsy monitoring intracranial electroencephalograph electrodes using MRI: Radiofrequency-induced heating”. In: *Journal of Magnetic Resonance Imaging: An Official Journal of the International Society for Magnetic Resonance in Medicine* 28.5 (2008), pp. 1233–1244.

[11] Xiangkun Chen and T Parks. “Design of FIR filters in the complex domain”. In: *IEEE Transactions on Acoustics, Speech, and Signal Processing* 35.2 (1987), pp. 144–153.

[12] Zsófia Clemens et al. “Fine-tuned coupling between human parahippocampal ripples and sleep spindles”. In: *European Journal of Neuroscience* 33.3 (2011), pp. 511–520.

[13] Ivan Cohen et al. “On the origin of interictal activity in human temporal lobe epilepsy in vitro”. In: *Science* 298.5597 (2002), pp. 1418–1421.

[14] M Corsi-Cabrera et al. “Power and coherent oscillations distinguish REM sleep, stage 1 and wakefulness”. In: *International Journal of Psychophysiology* 60.1 (2006), pp. 59–66.

[15] Nathan E Crone, Alon Sinai, and Anna Korzeniewska. “High-frequency gamma oscillations and human brain mapping with electrocorticography”. In: *Progress in brain research* 159 (2006), pp. 275–295.

[16] Anders M Dale, Bruce Fischl, and Martin I Sereno. “Cortical surface-based analysis: I. Segmentation and surface reconstruction”. In: *Neuroimage* 9.2 (1999), pp. 179–194.

[17] Heidi Danker-hopfe et al. “Interrater reliability for sleep scoring according to the Rechtschaffen & Kales and the new AASM standard”. In: *Journal of sleep research* 18.1 (2009), pp. 74–84.

[18] Arnaud Delorme and Scott Makeig. “EEGLAB: an open source toolbox for analysis of single-trial EEG dynamics including independent component analysis”. In: *Journal of neuroscience methods* 134.1 (2004), pp. 9–21.

[19] Arnaud Delorme et al. “From single-trial EEG to brain area dynamics”. In: *Neurocomputing* 44 (2002), pp. 1057–1064.

[20] Rahul S Desikan et al. “An automated labeling system for subdividing the human cerebral cortex on MRI scans into gyral based regions of interest”. In: *Neuroimage* 31.3 (2006), pp. 968–980.

[21] John S Duncan et al. “Adult epilepsy”. In: *The Lancet* 367.9516 (2006), pp. 1087–1100.

[22] Andrew R Dykstra et al. “Individualized localization and cortical surface-based registration of intracranial electrodes”. In: *Neuroimage* 59.4 (2012), pp. 3563–3570.

[23] Bradley J Edelman, Bryan Baxter, and Bin He. “EEG source imaging enhances the decoding of complex right-hand motor imagery tasks”. In: *IEEE Transactions on Biomedical Engineering* 63.1 (2015), pp. 4–14.

[24] B Fischl, MI Sereno, and AM Dale. “Cortical surface-based analysis-II: Inflation, flattening, and a surface-based coordinate system [WWW Document]”. In: *URL: http://discovery. ucl. ac. uk/145122/(accessed 9.21. 11)* (1999).

[25] Bruce Fischl. “FreeSurfer”. In: *Neuroimage* 62.2 (2012), pp. 774–781.

[26] Robert S Fisher et al. “Epileptic seizures and epilepsy: definitions proposed by the International League Against Epilepsy (ILAE) and the International Bureau for Epilepsy (IBE)”. In: *Epilepsia* 46.4 (2005), pp. 470–472.

[27] Patrick M Fuller, Joshua J Gooley, and Clifford B Saper. “Neurobiology of the sleep-wake cycle: sleep architecture, circadian regulation, and regulatory feedback”. In: *Journal of biological rhythms* 21.6 (2006), pp. 482–493.

[28] Bernard Gibaud. “The DICOM standard: a brief overview”. In: *Molecular imaging: computer reconstruction and practice* (2008), pp. 229–238.

[29] Thalía Harmony. "The functional significance of delta oscillations in cognitive processing". In: *Frontiers in integrative neuroscience* 7 (2013), p. 83.

[30] Suzana Herculano-Houzel. "The human brain in numbers: a linearly scaled-up primate brain". In: *Frontiers in human neuroscience* 3 (2009), p. 31.

[31] Desmond J Higham and Nicholas J Higham. *MATLAB guide*. SIAM, 2016.

[32] Jiang Hsieh. *Computed tomography: principles, design, artifacts, and recent advances*. Vol. 114. SPIE press, 2003.

[33] Conrad Iber et al. "The new Sleep Scoring Manual–The evidence behind the rules". In: *Journal of Clinical Sleep Medicine* 3.02 (2007), pp. 107–107.

[34] Bo Jin, Norman K So, and Shuang Wang. "Advances of intracranial electroencephalography in localizing the epileptogenic zone". In: *Neuroscience bulletin* 32.5 (2016), pp. 493–500.

[35] Mathias Johansson. "The hilbert transform". In: *Mathematics Master's Thesis. Växjö University, Suecia. Disponible en internet: http://w3. msi. vxu. se/exarb/mj_ex. pdf, consultado el* 19 (1999).

[36] Ali R Khan, Lei Wang, and Mirza Faisal Beg. "FreeSurfer-initiated fully-automated subcortical brain segmentation in MRI using large deformation diffeomorphic metric mapping". In: *Neuroimage* 41.3 (2008), pp. 735–746.

[37] Andrew L Ko and Chao-Hung Kuo. "Surgery for Temporal Lobe Epilepsy". In: *Principles of Neurological Surgery*. Elsevier, 2018, pp. 761–770.

[38] Abraham Kuruvilla and Roland Flink. "Intraoperative electrocorticography in epilepsy surgery: useful or not?" In: *Seizure* 12.8 (2003), pp. 577–584.

[39] Jean-Philippe Lachaux et al. “High-frequency neural activity and human cognition: past, present and possible future of intracranial EEG research”. In: *Progress in neurobiology* 98.3 (2012), pp. 279–301.

[40] Roan A LaPlante et al. “The interactive electrode localization utility: software for automatic sorting and labeling of intracranial subdural electrodes”. In: *International journal of computer assisted radiology and surgery* 12.10 (2017), pp. 1829–1837.

[41] Kenneth D Laxer et al. “The consequences of refractory epilepsy and its treatment”. In: *Epilepsy & behavior* 37 (2014), pp. 59–70.

[42] Aristidis Likas, Nikos Vlassis, and Jakob J Verbeek. “The global k-means clustering algorithm”. In: *Pattern recognition* 36.2 (2003), pp. 451–461.

[43] Geoffrey J McLachlan, Sharon X Lee, and Suren I Rathnayake. “Finite mixture models”. In: *Annual review of statistics and its application* 6 (2019), pp. 355–378.

[44] Naresh Nagabushan. “Analyzing and Classifying Neural Dynamics from Intracranial Electroencephalography Signals in Brain-Computer Interface Applications”. PhD thesis. Virginia Tech, 2019.

[45] M Nishida et al. “Prefrontal theta during REM sleep enhances emotional memory”. In: *Cerebral Cortex* 19 (2009), pp. 1158–1166.

[46] Satu Palva and J Matias Palva. “Functional roles of alpha-band phase synchronization in local and large-scale cortical networks”. In: *Frontiers in psychology* 2 (2011), p. 204.

[47] Aakash K Patel, Vamsi Reddy, and John F Araujo. “Physiology, sleep stages”. In: *StatPearls [Internet]* (2020).

[48] Douglas A Reynolds. “Gaussian Mixture Models.” In: *Encyclopedia of biometrics* 741 (2009), pp. 659–663.

[49] Perrine Ruby et al. “Alpha reactivity to complex sounds differs during REM sleep and wakefulness”. In: *PLoS One* 8.11 (2013), e79989.

[50] Simon Ruch et al. “Sleep stage II contributes to the consolidation of declarative memories”. In: *Neuropsychologia* 50.10 (2012), pp. 2389–2396.

[51] Pradeep Shenoy et al. “Generalized features for electrocorticographic BCIs”. In: *IEEE Transactions on Biomedical Engineering* 55.1 (2007), pp. 273–280.

[52] Athanassios G Siapas and Matthew A Wilson. “Coordinated interactions between hippocampal ripples and cortical spindles during slow-wave sleep”. In: *Neuron* 21.5 (1998), pp. 1123–1128.

[53] Rebecca Spencer. “Neurophysiological basis of sleep’s function on memory and cognition”. In: *ISRN Physiology* 2013 (2013).

[54] William O Tatum IV. *Handbook of EEG interpretation*. Demos Medical Publishing, 2014.

[55] D Terman, A Bose, and N Kopell. “Functional reorganization in thalamocortical networks: Transition between spindling and delta sleep rhythms”. In: *Proceedings of the National Academy of Sciences* 93.26 (1996), pp. 15417–15422.

[56] István Ulbert et al. “Multiple microelectrode-recording system for human intracortical applications”. In: *Journal of neuroscience methods* 106.1 (2001), pp. 69–79.

[57] Sujith Vijayan et al. “Frontal beta-theta network during REM sleep”. In: *Elife* 6 (2017), e18894.

[58] Sujith Vijayan et al. “Thalamic mechanisms underlying alpha-delta sleep with implications for fibromyalgia”. In: *Journal of Neurophysiology* 114.3 (2015), pp. 1923–1930.

[59] Jim Waterhouse, Yumi Fukuda, and Takeshi Morita. “Daily rhythms of the sleep-wake cycle”. In: *Journal of physiological anthropology* 31.1 (2012), pp. 1–14.

[60] Sabrina L Wendt et al. “Inter-expert and intra-expert reliability in sleep spindle scoring”. In: *Clinical Neurophysiology* 126.8 (2015), pp. 1548–1556.

[61] Catherine Westbrook and John Talbot. *MRI in Practice*. John Wiley & Sons, 2018.

[62] Dominik Zumsteg and Heinz Gregor Wieser. “Presurgical evaluation: current role of invasive EEG”. In: *Epilepsia* 41 (2000), S55–S60.

.

Appendices

Appendix A

Hypnograms

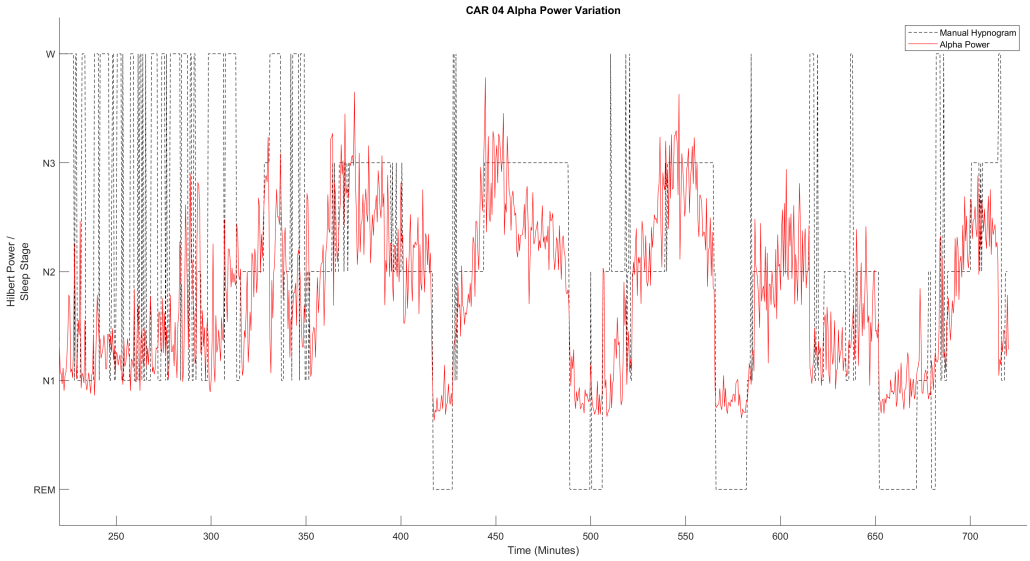

Figure A.1: Alpha Power Variation and Hypnogram for Patient CAR 04

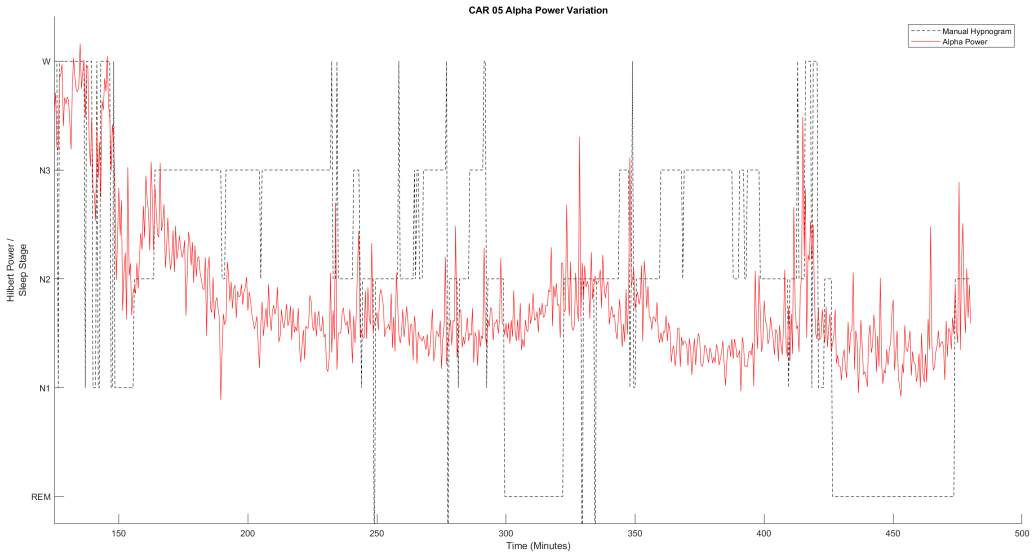

Figure A.2: Alpha Power Variation and Hypnogram for Patient CAR 05

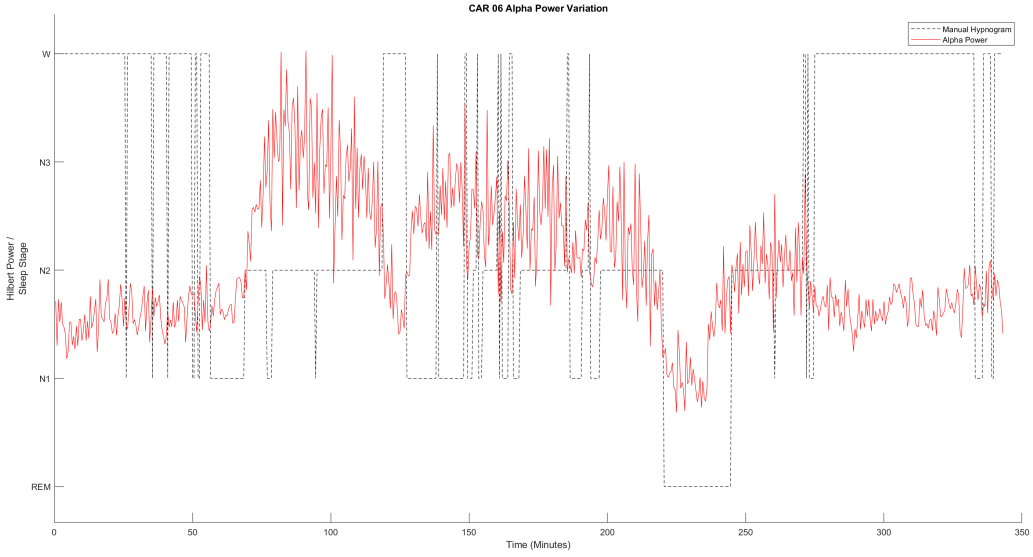

Figure A.3: Alpha Power Variation and Hypnogram for Patient CAR 06

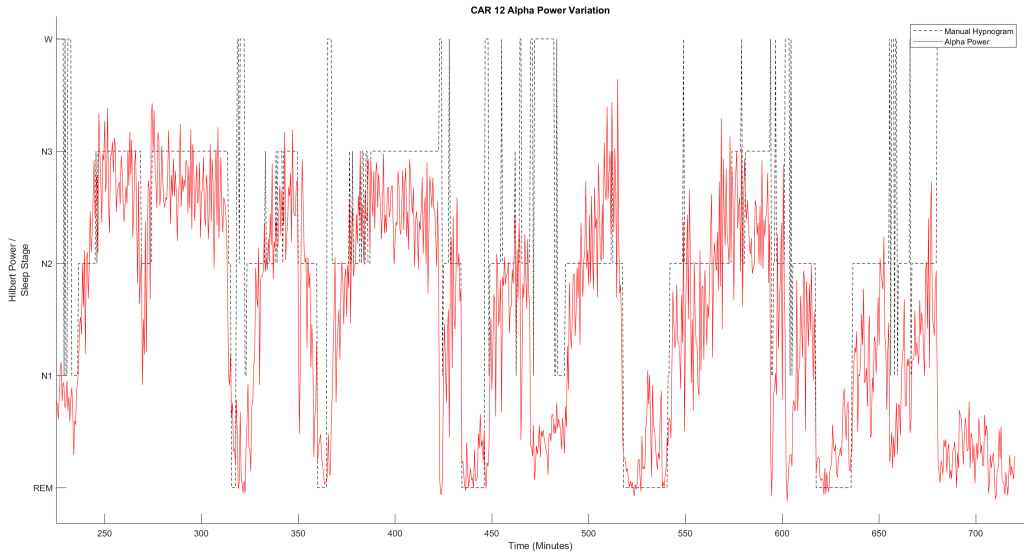

Figure A.4: Alpha Power Variation and Hypnogram for Patient CAR 12

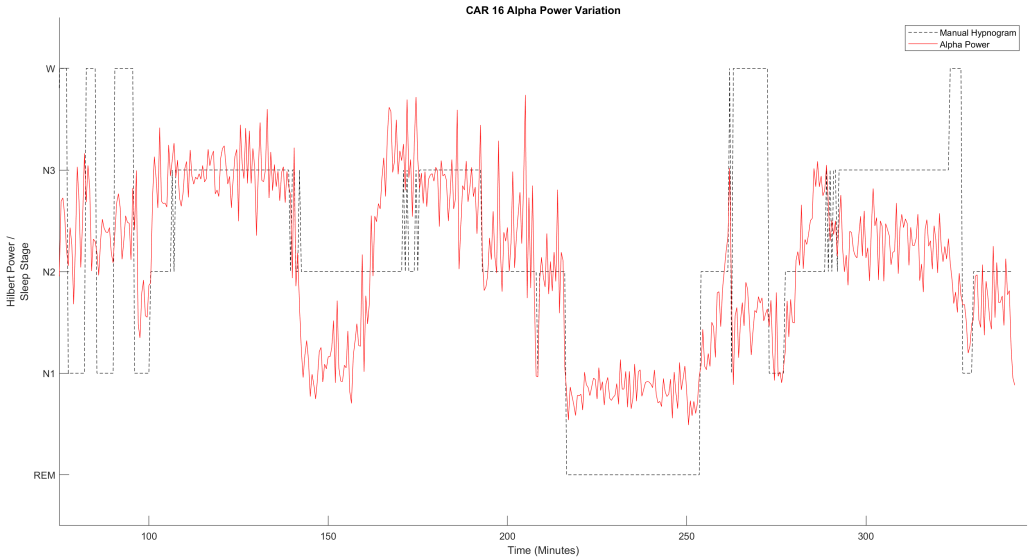

Figure A.5: Alpha Power Variation and Hypnogram for Patient CAR 16

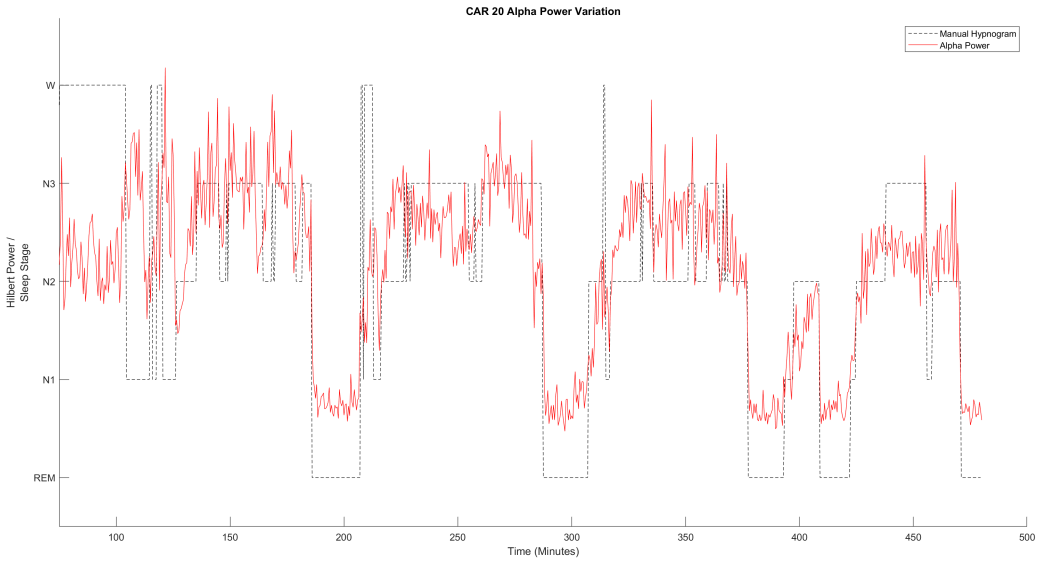

Figure A.6: Alpha Power Variation and Hypnogram for Patient CAR 20

Appendix B

Distributions and Fits

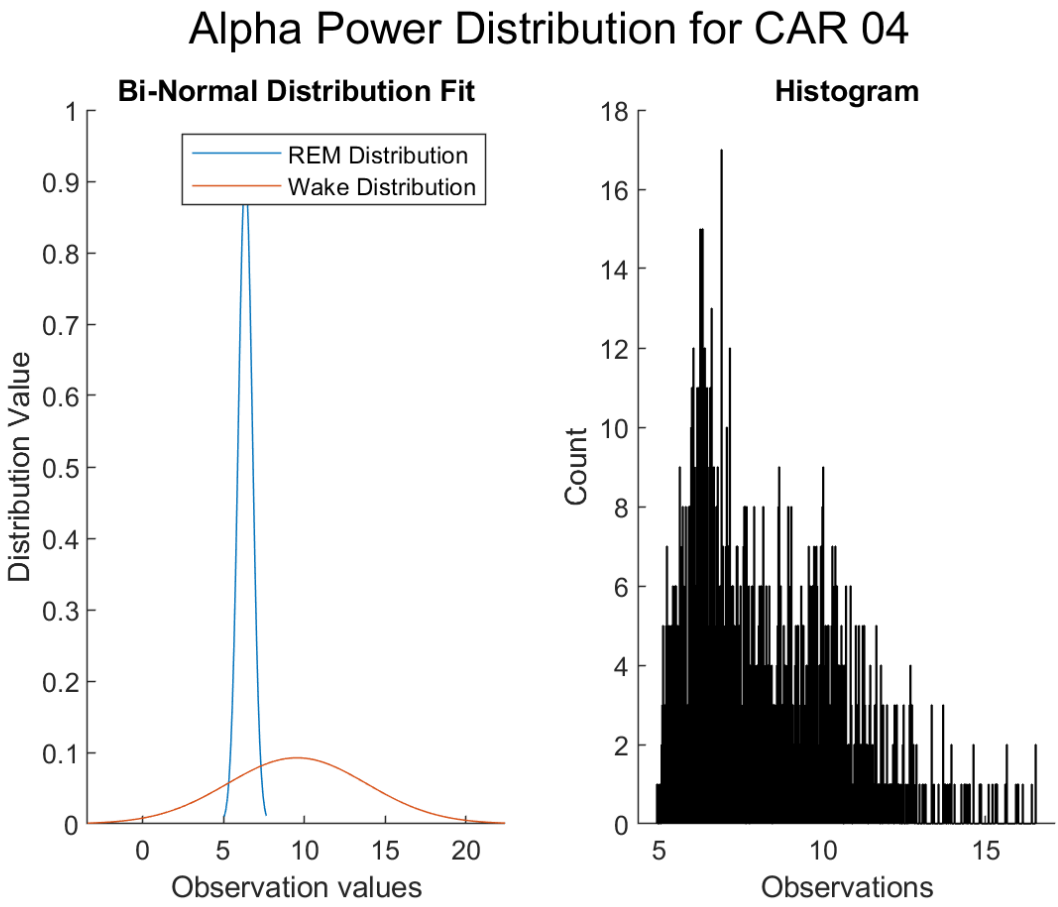

Figure B.1: Power distribution and Binormal Fit for Patient CAR 04

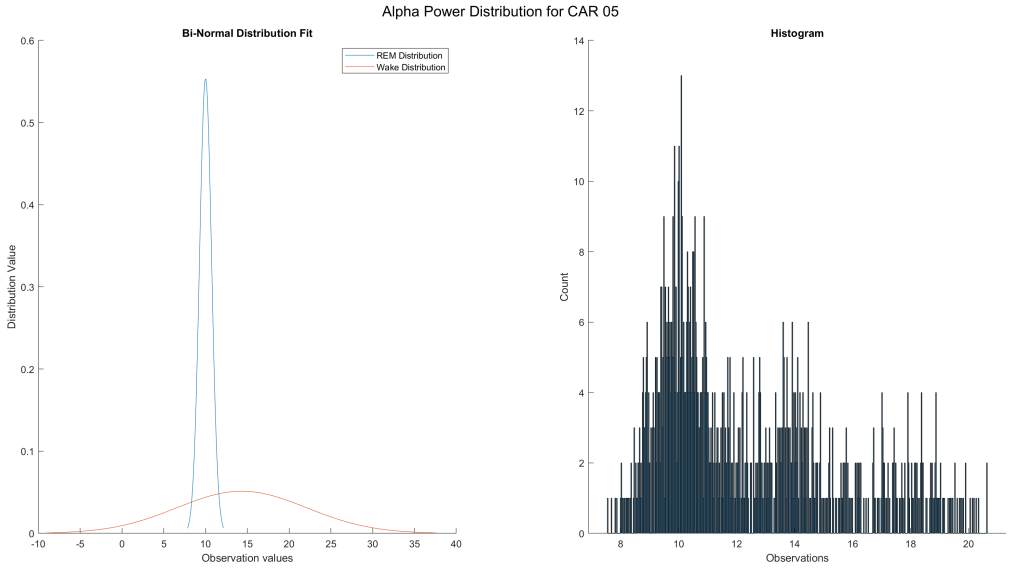

Figure B.2: Power distribution and Binormal Fit for Patient CAR 05

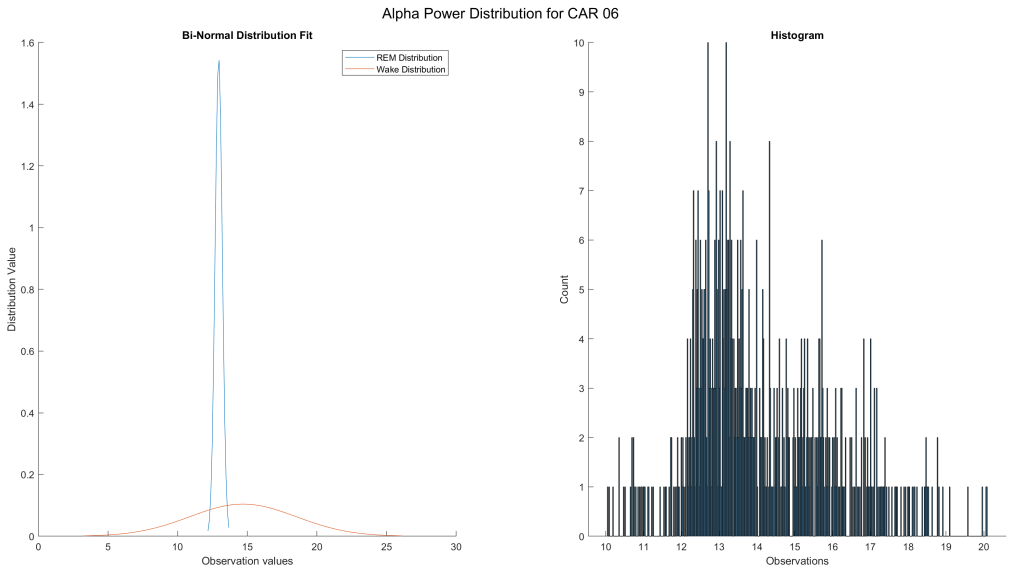

Figure B.3: Power distribution and Binormal Fit for Patient CAR 06

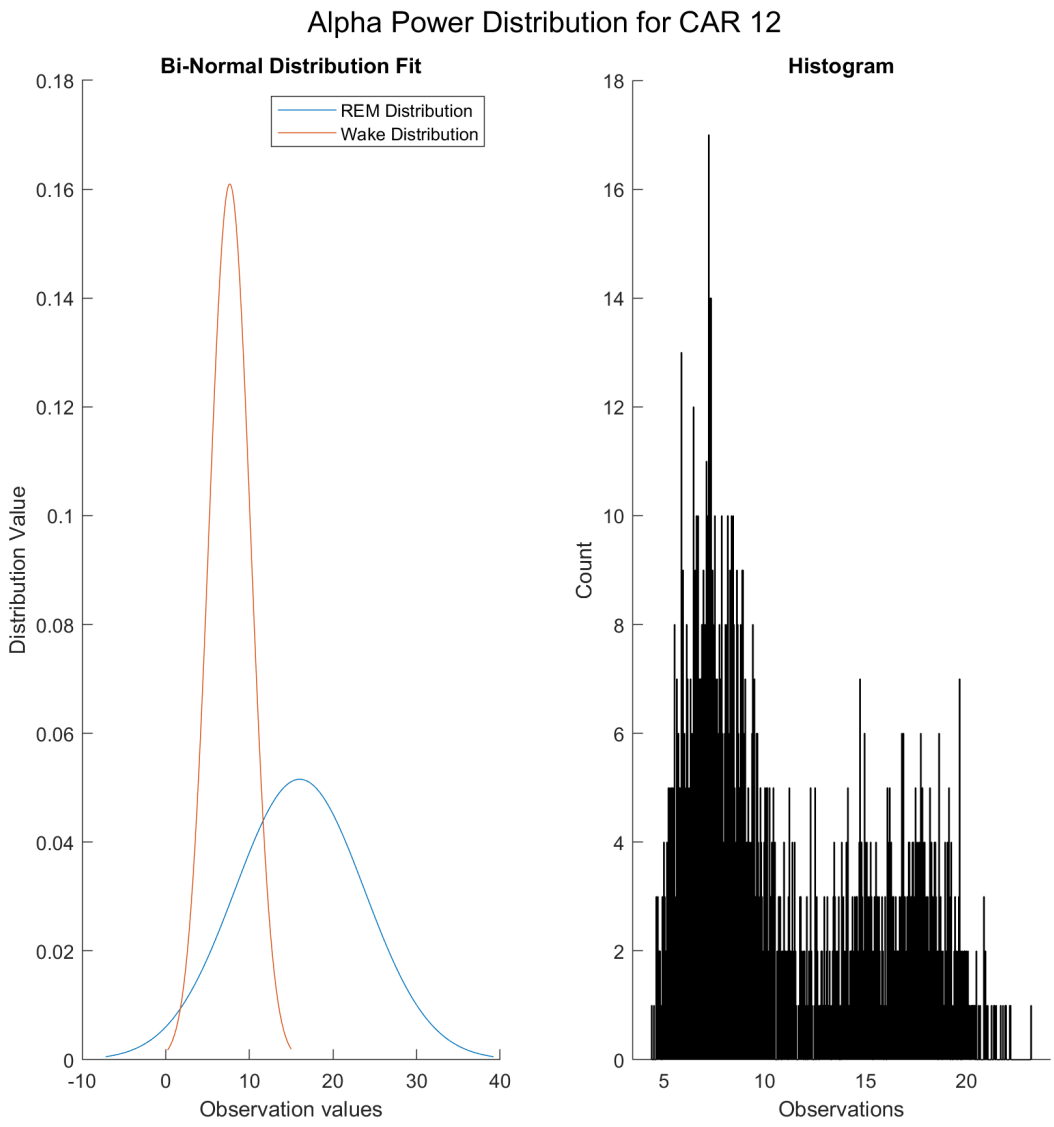

Figure B.4: Power distribution and Binormal Fit for Patient CAR 12

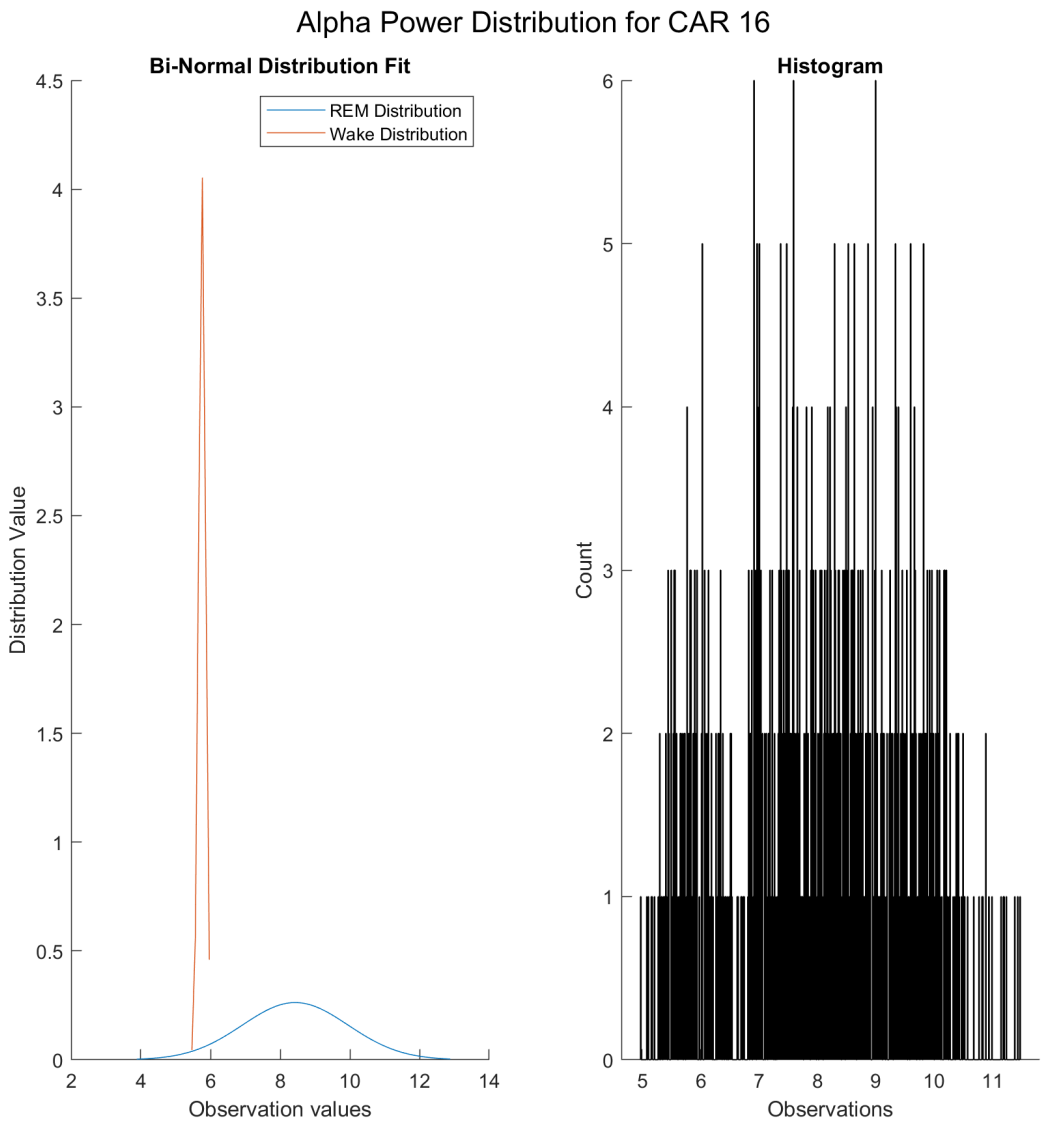

Figure B.5: Power distribution and Binormal Fit for Patient CAR 16

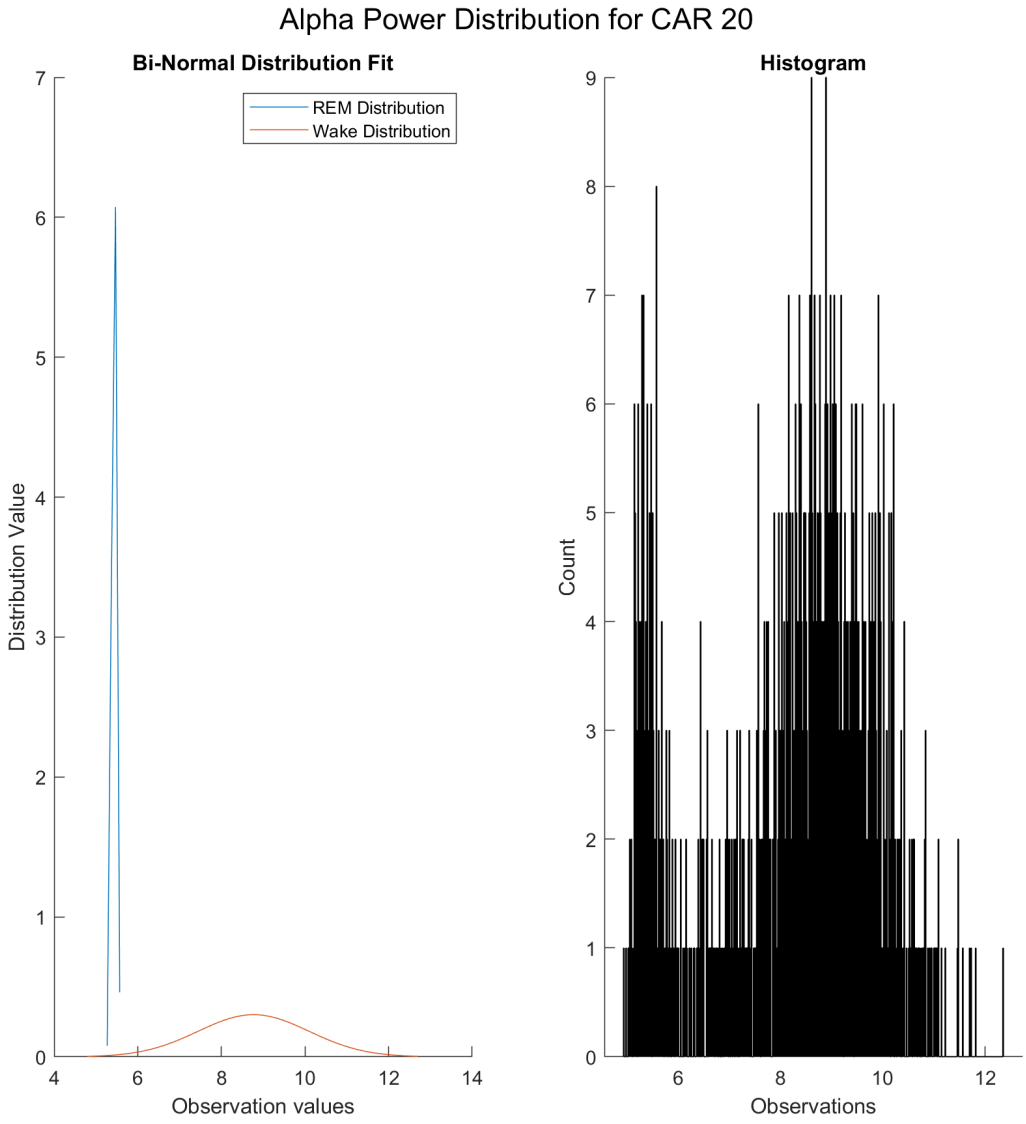

Figure B.6: Power distribution and Binormal Fit for Patient CAR 20

SUBJECT	Accuracy for Wake vs. REM Classification (%)	
Threshold used:	*Mean + 1 Standard deviation*	*Mean + 2 Standard deviations*
CAR 04	91.34	87.95
CAR 05	78.21	72.25
CAR 06	66.03	81.27
CAR 12	42.16	81.95
CAR 16	93.00	82.88
CAR 20	87.46	97.13

Figure B.7: Wake - REM Scoring accuracy using two different thresholds

Appendix C

Channel Information

Locations denoted with '' are the closest gray matter regions for their corresponding channels because these channels were found to lie in the white matter.*

Channel Name	Anatomical Location
'AHipp-3Ld7'	ctx_lh_S_temporal_sup*
'Amg-1Ld7'	ctx_lh_S_orbital_med-olfact*
'Amg-2Rd7'	ctx_rh_S_temporal_sup*
'FOGM-11Ld11'	ctx_lh_S_front_sup
'FOGM-12Rd11'	ctx_rh_G_front_middle*
'FP-16Rd11'	ctx_rh_S_front_middle
'HippM-5Ld10'	ctx_lh_G_temporal_middle
'HippM-6Rd8'	ctx_rh_G_temporal_inf
'IFCG-13Ld7'	ctx_lh_S_front_middle*
'PHipp-8Rd9'	ctx_rh_G_temporal_middle
'SFOG-10Rd11'	ctx_rh_S_front_sup
'SFOG-9Ld11'	ctx_lh_G_front_sup

Figure C.1: Channel information for Patient CAR 04

Channel Name	Anatomical Location
'AHipp-3Ld7'	ctx_lh_S_temporal_sup
'AHipp-4Rd7'	ctx_rh_S_temporal_sup*
'Amg-1Ld7'	ctx_lh_S_temporal_sup
'Amg-2Rd7'	ctx_rh_G_temp_sup-Plan_polar
'FOGM-11Ld11'	ctx_lh_G_front_sup
'FOGM-12Rd10'	ctx_rh_G_front_middle
'FP-15Ld11'	ctx_lh_G_front_middle
'HippM-5Ld7'	ctx_lh_G_temporal_middle*
'HippM-6Rd9'	ctx_rh_G_temporal_middle

Figure C.2: Channel information for Patient CAR 05

Channel Name	Anatomical Location
'AHipp-3Ld6'	ctx_lh_S_temporal_sup
'AHipp-4RT6'	ctx_rh_S_temporal_sup
'Amg-1Ld5'	ctx_lh_S_circular_insula_inf
'Amg-2RT8'	ctx_rh_S_temporal_sup
'LIFCG-13Ld5'	ctx_lh_G_and_S_frontomargin
'LMFG-11Ld8'	ctx_lh_G_front_middle
'LSFG-9Ld12'	ctx_lh_G_front_sup
'RIFCG-14RT5'	ctx_rh_G_and_S_cingul-Ant*
'RMFFP-16RT7'	ctx_rh_S_front_middle
'RMFG-12RT9'	ctx_rh_G_front_middle

Figure C.3: Channel information for Patient CAR 06

Channel Name	Anatomical Location
'AHipp-4Rd5'	ctx_rh_S_collat_transv_ant*
'AHipp-4Rd6'	ctx_rh_S_temporal_inf*
'IFCG-14Rd5'	ctx_rh_S_circular_insula_sup*
'IFCG-14Rd6'	ctx_rh_Lat_Fis-ant-Horizont*
'MFOG-12Rd7'	ctx_rh_S_front_middle*
'MFOG-12Rd8'	ctx_rh_G_front_middle*
'SFGR-10Rd8'	ctx_rh_S_front_middle*
'SFGR-10Rd9'	ctx_rh_S_front_middle*
'SFGR-9Ld10'	ctx_lh_G_front_sup
'SFGR-9Ld11'	ctx_lh_G_front_sup
'SFGR-9Ld8'	ctx_lh_G_front_sup
'SFGR-9Ld9'	ctx_lh_G_front_sup

Figure C.4: Channel information for Patient CAR 12

Channel Name	Anatomical Location
'AHipp-3Ld5'	ctx_lh_S_collat_transv_ant*
'AHipp-4Rd5'	ctx_rh_S_temporal_sup*
'Amg-1Ld5'	ctx_rh_S_circular_insula_inf
'Amg-2Rd5'	ctx_rh_S_circular_insula_inf
'IFCG-13Ld5'	ctx_lh_S_front_inf*
'IFCG-14Rd5'	ctx_rh_S_front_middle*
'MFOG-11Ld11'	ctx_lh_G_front_middle*
'MFOG-11Ld9'	ctx_lh_G_front_middle*
'MHipp-5Ld5'	ctx_rh_S_temporal_sup*
'MHipp-6Rd5'	ctx_rh_S_temporal_sup
'PHipp-7Ld9'	ctx_lh_G_temporal_middle*
'SFOG-10Rd5'	ctx_rh_G_and_S_cingul-Ant*
'SFOG-9Ld5'	ctx_lh_G_and_S_cingul-Ant*

Figure C.5: Channel information for Patient CAR 16

Channel Name	Anatomical Location
'AHipp-3Ld5'	ctx_rh_S_temporal_inf*
'AHipp-4Rd5'	ctx_rh_S_collat_transv_ant*
'AHipp-4Rd6'	ctx_rh_S_temporal_inf*
'Amg-2Rd6'	ctx_rh_S_temporal_sup*
'IFCG-13Ld4'	ctx_lh_S_orbital-H_Shaped*
'IFCG-14Rd4'	ctx_rh_G_and_S_cingul-Ant*
'MFOG-11Ld11'	ctx_lh_G_front_middle
'MHipp-5Ld5'	ctx_lh_S_temporal_sup*
'MHipp-5Ld6'	ctx_lh_S_temporal_inf*
'MHipp-6Rd5'	ctx_rh_S_temporal_sup
'SFGR-10Rd9'	ctx_rh_G_front_sup*
'SFGR-9Ld13'	ctx_lh_G_front_sup

Figure C.6: Channel information for Patient CAR 20